CHAPTER IX

VORTEX RINGS OF ONE FLUID IN ANOTHER IN FREE FALL

IX. 1 Introduction
IX. 2 Classical Vortex Rings
IX. 3 The Normal Stress Balance
IX. 4 Stokes Flow Around a Drop
IX. 5 Dimensionless Parameters
IX. 6 Physical and Other Properties
IX. 7 Distortion of the Spherical Drop
IX. 8 Formation of Rings
IX. 9 Two-Fluid Systems That Do and Do Not Form Vortex Rings

IX.1 INTRODUCTION

In this chapter, we present and interpret experiments in which vortex rings of one immiscible liquid are created in another from drops falling from rest under gravity. These rings are associated with circulations generated by viscosity and, unlike classical vortex rings (which are associated with high Reynolds number flow of miscible fluids), they can exist even at very low Reynolds numbers. Since the rings do not diffuse, they are well-defined. Nonetheless, there are many similarities in the dynamics of formation and flow of miscible and immiscible rings. We are going to identify parameters which appear to correlate our observations and to show photographs of some of the more interesting things we have seen. The data for the experiments were collected and reduced by Nick Baumann, and he and Paul Mohr did the photography.

IX.2 CLASSICAL VORTEX RINGS

By way of comparison, it is instructive to recall that in classical hydrodynamics, it is usual to consider vortical regions embedded in an otherwise irrotational flow. In the case of the ring, a cross-section (figure 2.1(a)) is like the "potential vortex" (figure 2.1 (b)): the flow outside a cylinder which rotates rigidly. This is the Taylor problem (flow between two concentric cylinders with the inner one rotating and the outer one fixed) with the outer cylinder moved to infinity. The streamfunction ψ of the flow, with $(\psi_y, -\psi_x)$ for the velocity in the $x-y$-plane, and $r = (x^2 + y^2)^{1/2}$, is then $\psi = c\ ln\ r$. Thus, $\Delta\psi = 0$ and the flow is irrotational. The potential vortex satisfies the no slip boundary condition at the cylindrical boundary, and it is one of only a few potential flow solutions of the Navier-Stokes equations.

In the classical theory of vortex rings, viscosity is absent, diffusion is absent and surface tension is absent. For the classical case, we think of a smoke ring. Many beautiful photographs of vortex rings in miscible liquids can be found in the photograph album of Van Dyke [1982].

Vortex rings can be generated in a number of ways. One way is to impulsively eject a puff of fluid from a circular opening into a bath of the same fluid, as in the smoke ring [Baird, Wairegi and Loo 1977]. Another is to let a drop of liquid fall into a pool of the same liquid [Chapman and Critchlow 1967]. A third method is to force a buoyant fluid into a tank of water (see section 6.3.2 of Turner [1979]) [Simons and Larson 1974]. These experiments do not involve immiscible liquids. Rings are more easily created in miscible rather than immiscible liquid. Thomson and Newall [1885] did an interesting study of ring formation and their stability in miscible and immiscible liquids. They say that

> It is not every liquid, however, which, when dropped into water, gives rise to rings, for if we drop into water any liquid which does not mix with it, such as chloroform, the drop in consequence of the surface tension remains spherical as it descends. In fact, we may say that, with some few exceptions to be noticed later, rings are formed only when a liquid is dropped into one with which it can mix. This is important, because surface tension has been supposed to play an important part in the formation of these rings; it is difficult, however, to see how any appreciable surface tension can exist between liquids that can mix, and as far as our experiments go they tend to show that it is only the absence of surface tension which is necessary for their production. There are, as we shall show later, many cases where rings are formed under circumstances in which there is no possibility of capillary action, such as when the liquid into which the drop falls is the same as the drop itself.

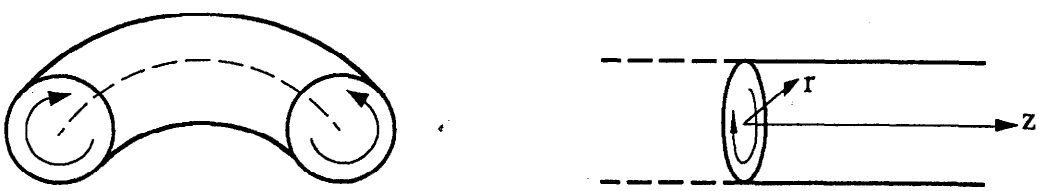

(a) (b)

Figure 2.1 (a) The two circular cross-sections of a ring vortex are shown. The flow is as indicated. The dashed line denotes the axis at the center of the ring. The ring as a whole turns about this axial line. The continual turning of the ring is analogous to the rigid-body rotation of a straight cylinder shown in (b) if the ring were cut and straightened. (b) An infinitely long solid cylinder is rotating with azimuthal velocity Ωr, where Ω is the angular speed. The flow outside the cylinder is irrotational and given by the streamfunction $\psi = c \ln r$.

Most of the experimental studies of vortex rings are for rings generated impulsively or otherwise in a single fluid or between miscible liquids. Most of the theoretical studies proceed from the inviscid equations of motion in which the vorticity is confined to certain regions, say rings, in an otherwise potential flow. These are models of flow at high Reynolds numbers. Low Reynolds number studies of the settling and break-up of miscible drops and the formation of rings have been given by Kojima, Hinch and Acrivos [1984] (figure 2.2) and by Arecchi, Buah-Bassuah, Francini, Pérez-Garcia and Quercioli [1989] (figure 2.3). To explain the discrepancies between their experimental observations and their Stokes flow calculations, Kojima et al introduced some notions of transient interfacial tension. We are going to consider this notion in more detail in chapter X.

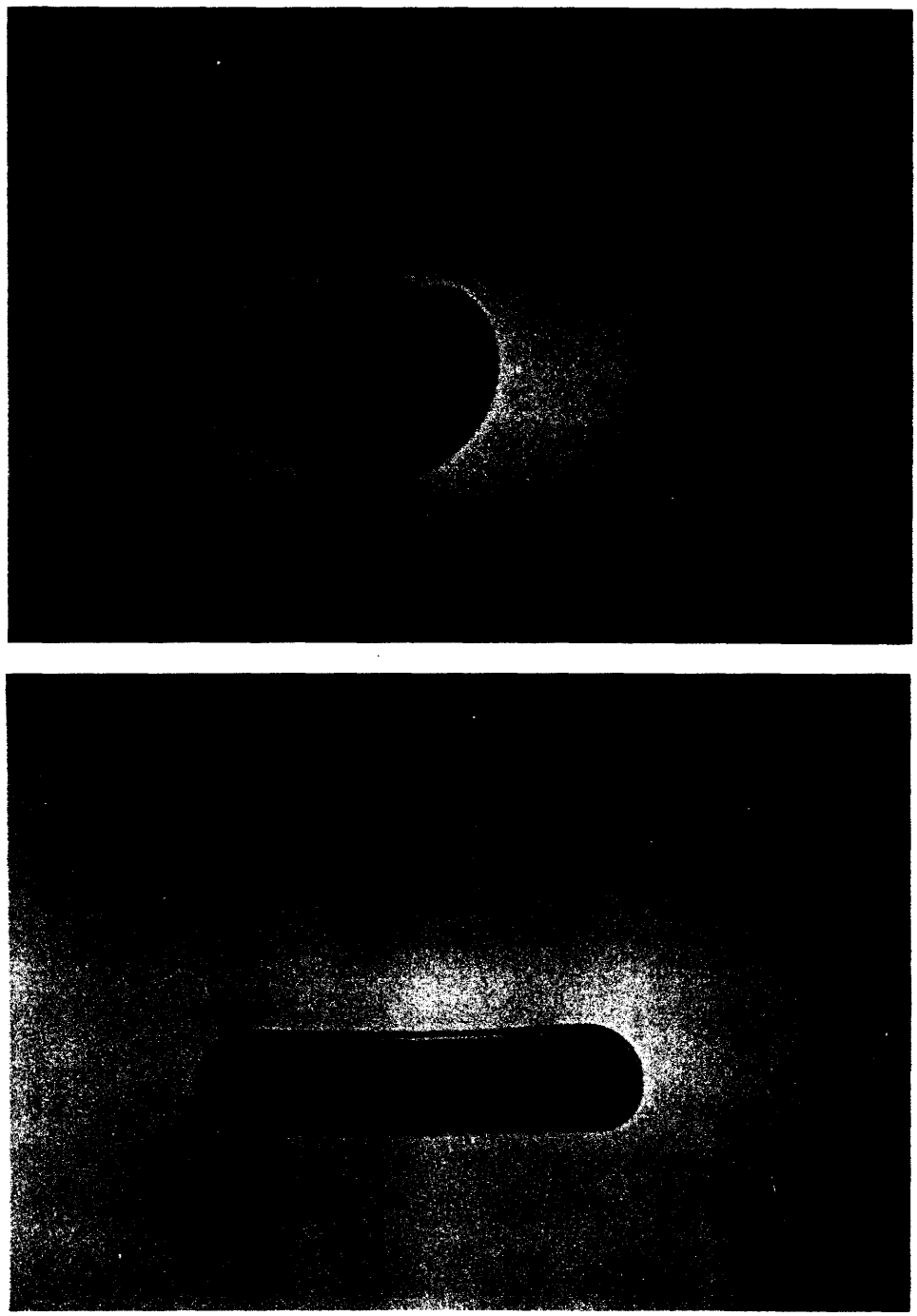

Figure 2.2 (After Kojima, Hinch and Acrivos [1984]). Falling drops of aqueous corn syrup of density 1.329 g/cm^3 and viscosity 3.9 P into aqueous corn syrup of density 1.26 g/cm^3 and viscosity 0.51 P. (a) The low viscosity mixture intrudes into the drop at the trailing edge near the tail. (b) A vortex ring forms. (continued)

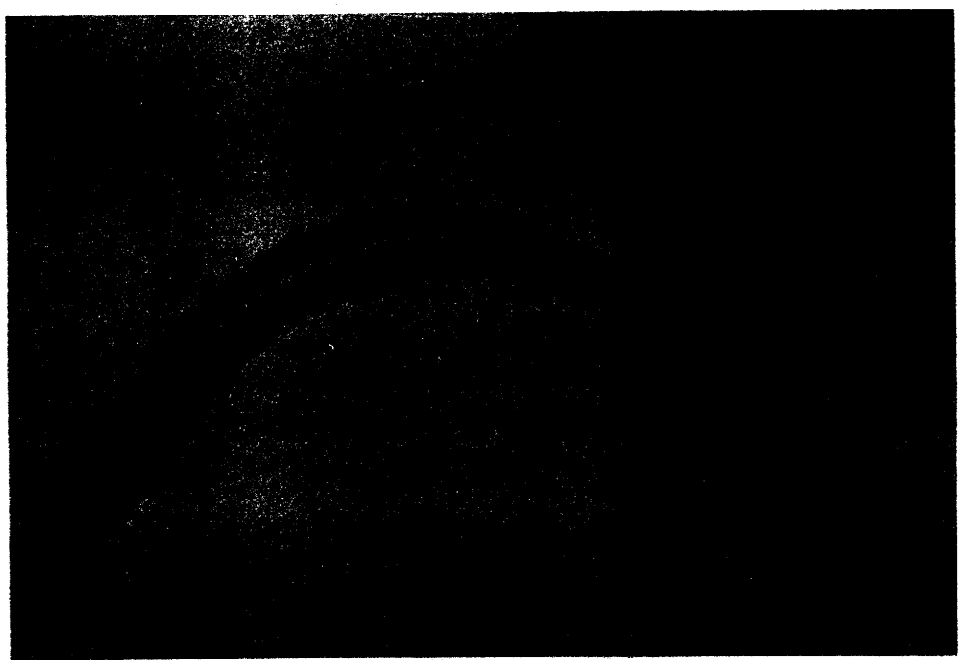

(c)

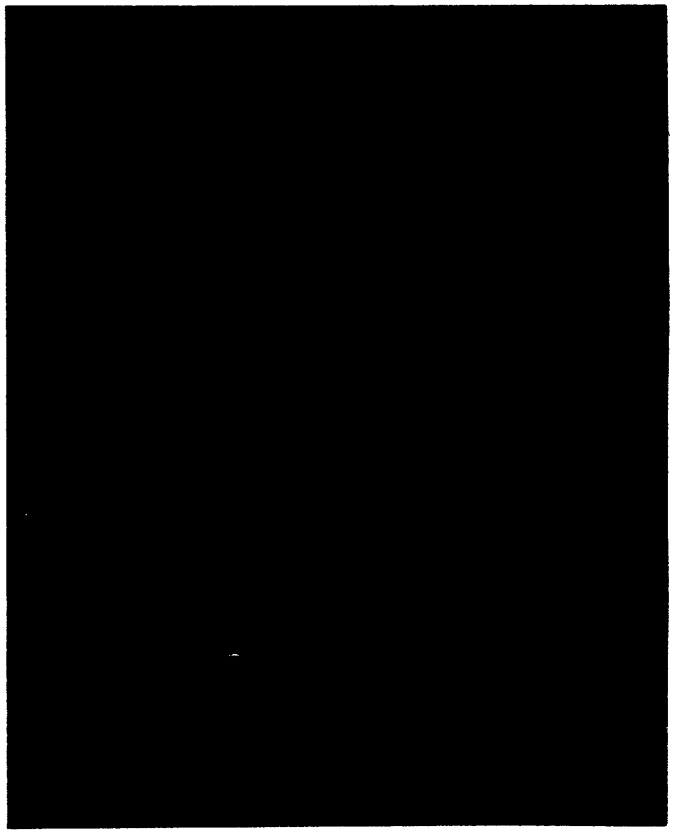

(d)

(c) Vortex ring (Rayleigh-Taylor) instability. (d) Cascade of new rings begins to form.

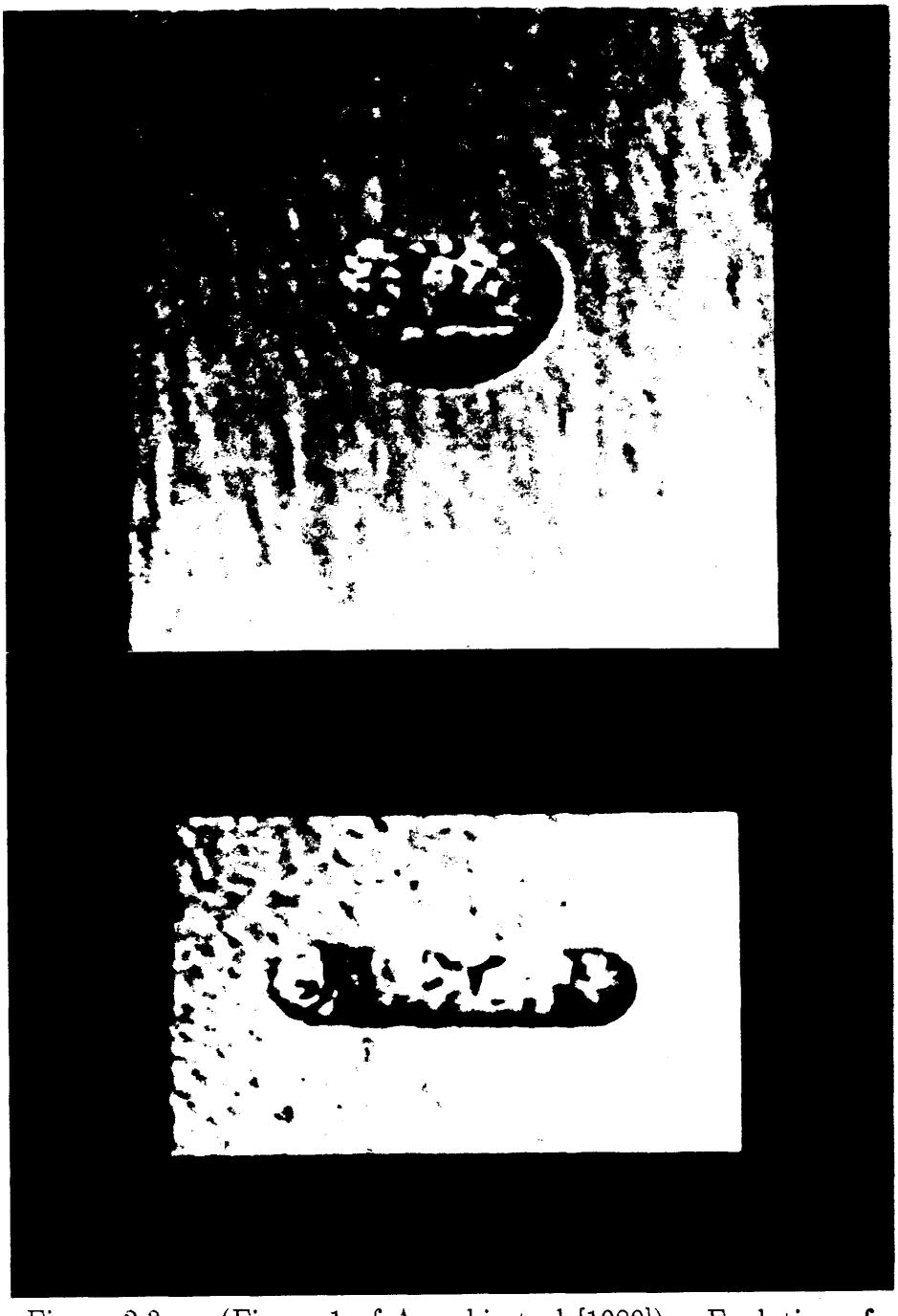

Figure 2.3 (Figure 1 of Arecchi et al [1989]) Evolution of a falling liquid drop with $r = 0.29$ cm and $\Delta\rho = 0.0789$ g/cc. (a) - (d) is a sequence of lateral views of the drop motion taken at the following positions from the free surface and times from the deposition: (a) 6.0 cm, 3.03 s; (b) 10.0cm, 5.2s; (c) 13.0 cm, 7.34s; and (d) 16.0 cm, 10.0 s. (c) shows the appearance of the turban instability (the change of sign in the curvature of the bottom membrane is the onset of what is called a turban instability, since the deformed drop looks like a turban), and (d) the torus breaking by Rayleigh-Taylor instability.

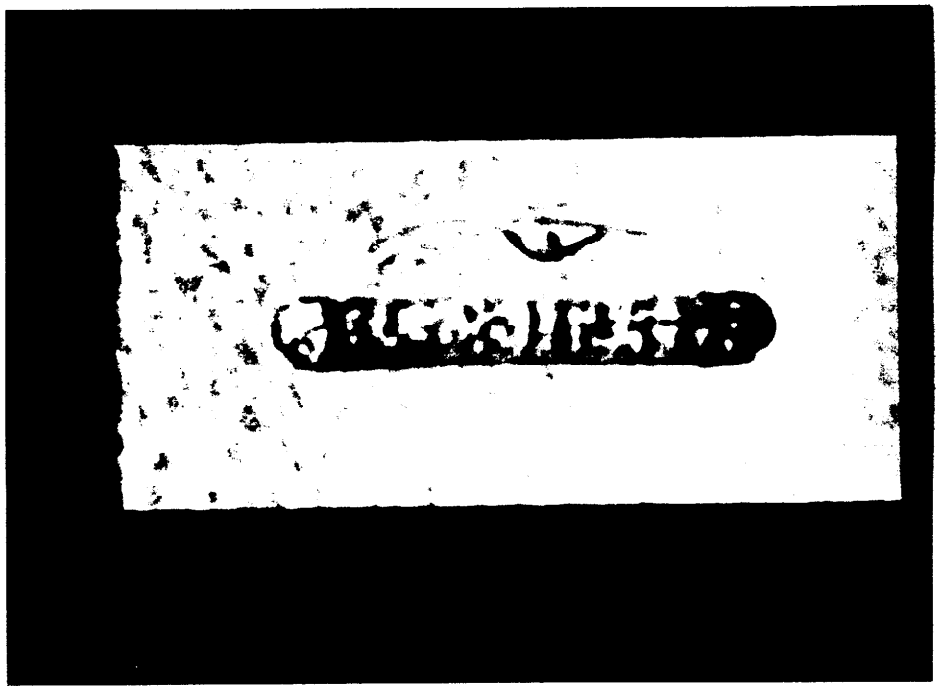

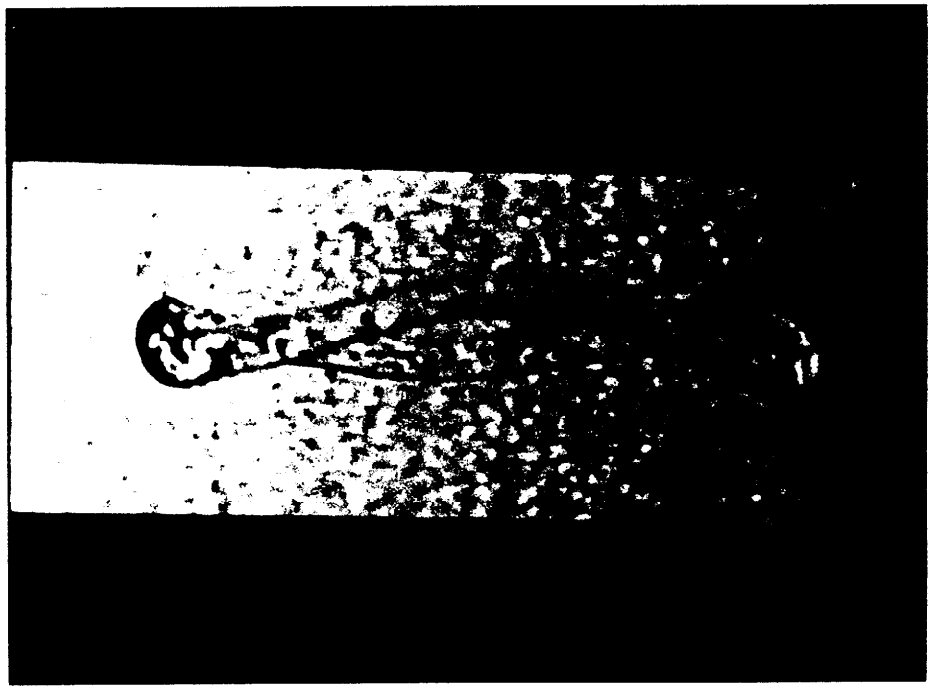

(c) (d)

Most of the studies of vortex rings in immiscible liquids are for water and air at high Reynolds numbers. One example is to let a bubble of air rise through water [Walters and Davidson 1963; Pedley 1968], and another is to let a drop of water fall through the air [O'Brien 1961]. The latter method leads to large deformations from the original drop, and the formation of bags which look very different from rings even though these are related. In the former study, it is necessary to inject the air impulsively to create a strong circulation in order to get a ring to form. A recent analysis of this problem has been given by Lundgren and Mansour [1990].

Stuke [1954] did experiments like those reported in this chapter. He mentions that prior to his work, the formation and break-up of immiscible rings happened too fast to be photographed with the technology that was available at that time. Stuke cites the work of Northrup [1912] who used paraffin in a water bath, where interfacial tension is large. Northrup needed to inject the paraffin at high speed so that viscous forces would create a circulation of sufficient magnitude, as in the case of air injected into water. The larger the interfacial tension, the faster the intrusive speed necessary to create a ring. Stuke showed that rings would form at slower speeds when water was replaced with amyl alcohol, with a consequent lowering of interfacial tension. The slower speeds allowed these processes to be recorded in photographs which can be compared with the photographs of this chapter. Initially, there is a membrane across the hole of the ring (cf. figures 8.1, 8.2). and then the membrane ruptures. Once formed, the ring starts to expand rapidly and the bulk of the paraffin flows into two or three bulges around the ring (cf. figures 8.3 (f), 8.4). These heavier bulges fall faster, so that the ring bends and breaks into two or three drops (see his figure 5, figure 2b of O'Brien [1961] and our figures). If a drop were large enough, it would form another vortex ring and the sequence repeats itself. An analogous description of the ring instability for miscible liquids at slow speed is given by Kojima et al [1984] for their figure 4 and by Arecchi et al [1989].

On the whole, it is not surprising that a phenomenon which occurs at zero interfacial tension also occurs at small values of interfacial tension. And *small* here means *with respect to viscous effects*, so that the actual numerical value of the coefficient of interfacial tension does not have to be small. The processes are similar whether miscible or immiscible liquids are involved, up to the ring stage. However, interfacial tension does affect the break-up pattern: for example [O'Brien 1961], it can prevent the smaller-sized drops from repeating the sequence of ring formation and break-up: this limits the vortex-cascade (Thomson and Newall [1885] describe this cascade for the case of an ink drop in water, with their figures 1 and 2 as illustrations) to one or two stages. Membrane *rupture* is another form of break-up. The rupture strength or breaking strength of membranes is not well-understood but it may be related to surface tension. We know that the rupture strength generally decreases with surface tension. When the surface tension parameter is small but the surface tension is large, a vortex ring spanned by a tough permanent membrane can form. In other cases in which interfacial tension has been reduced by surfactants, the membrane is blown out and an unstable vortex ring of the type shown in our photographs forms. The difference between strong and weak interfacial tension is illustrated in figures 7.5 and 8.3. In figure 7.5, a smaller drop of 1000 cS silicone oil is sucked into the wake of an oblate ring-like cap of the same silicone oil falling in a contaminated soy bean oil. The membrane in this system

is too tough to break. On the other hand, if a surfactant (97 % dye, 3% Rhodamine B base powder, Aldrich Chem. Co., Milwaukee, WI) is added (as in figure 8.3) the membrane breaks readily. Figure 2.3 (e) illustrates this well. The existence of a spanning membrane in miscible liquids is hard to understand without invoking the idea of transient interfacial tension induced by momentarily strong gradients of composition.

IX.3 THE NORMAL STRESS BALANCE

It is probable that the parameters which control the deformations of drops to rings in free fall are associated with the stress balance at the interface:

$$-[\![p]\!]\mathbf{n} + 2[\![\mu \mathbf{D}[\mathbf{u}]]\!]\mathbf{n} + S^*\mathbf{n}2H = 0, \tag{3.1}$$

where H is the mean curvature at a point on the interface Σ and

$$2H = \frac{1}{R_1} + \frac{1}{R_2}, \qquad \mathbf{D}[\mathbf{u}] = \frac{1}{2}(\nabla\mathbf{u} + (\nabla\mathbf{u})^T),$$

where R_1 and R_2 are the local radii of curvature at a point of Σ; $\mathbf{n}$ is the outward normal on the interface.

We denote

$$[\![\cdot]\!] = (\cdot)_d - (\cdot)_o,$$

to be the jump in the quantity $\cdot$ across the interface, where the subscript d stands for drop and o stands for the outer fluid. In the equilibrium case (that is, no flow), the drop or bubble pulls into a sphere with radius $R_1 = R_2 = a$ and equilibrium pressures satisfying

$$[\![p^e]\!] = p_d^e - p_o^e = \frac{2S^*}{a}.$$

Equation (3.1) may be decomposed into normal and tangential parts. The tangential part says that shear stress is continuous. By using the condition that the velocity is continuous at the interface

$$[\![\mathbf{u}]\!] = 0 \tag{3.2}$$

and the continuity equation, we will show that

$$[\![D_{nn}]\!] = 0, \tag{3.3}$$

where we denote

$$D_{nn} = \mathbf{n} \cdot \mathbf{D}[\mathbf{u}] \cdot \mathbf{n}.$$

This result will be used in equations (3.8) and (4.4).

For the proof, we write the continuity equation

$$\nabla \cdot \mathbf{u} = (\mathbf{n}\frac{\partial}{\partial n} + \nabla_{\|}) \cdot \mathbf{u} = 0 \tag{3.4}$$

where $\partial/\partial n = \mathbf{n}\cdot\nabla$, $\nabla_\parallel$ is the surface gradient $\mathbf{t_1}(\mathbf{t_1}\cdot\nabla)+\mathbf{t_2}(\mathbf{t_2}\cdot\nabla)$, and $\mathbf{t_1}$ and $\mathbf{t_2}$ are the two tangents to the interface. Then on the interface,

$$0 = [\![\nabla\cdot\mathbf{u}]\!] = [\![\mathbf{n}\cdot\frac{\partial\mathbf{u}}{\partial n}+\nabla_\parallel\cdot\mathbf{u}]\!]$$

$$= [\![\mathbf{n}\cdot\frac{\partial\mathbf{u}}{\partial n}]\!]+\nabla_\parallel\cdot[\![\mathbf{u}]\!]$$

$$= [\![\mathbf{n}\cdot\frac{\partial\mathbf{u}}{\partial n}]\!]. \tag{3.5}$$

We note next that

$$D_{nn} = n_i\frac{\partial u_i}{\partial x_j}n_j = \mathbf{n}\cdot\frac{\partial\mathbf{u}}{\partial n}. \tag{3.6}$$

We take the jump of (3.6) and use (3.5) to prove (3.3).

The next step in the reduction of the normal component of the stress balance on Σ is the decomposition of the pressure into an equilibrium part p^e, a hydrostatic part $p^s = \rho g z$, with $p^s = \rho_d g z$ in the drop, and a dynamic part Π due to the motion. We use a coordinate system where the origin is the center of the spherical drop, and we denote the parametrization for the surface of the drop by $z = z_\Sigma(x,y)$. Thus, $[\![p^s]\!] = [\![\rho]\!] g z_\Sigma$, and

$$[\![p]\!] = [\![p^e]\!]+[\![p^s]\!]+[\![\Pi]\!]$$

$$= \frac{2S^*}{a}+[\![\rho]\!] g z_\Sigma+[\![\Pi]\!]. \tag{3.7}$$

Combining now (3.3) and (3.7) with (3.1), we find that

$$-[\![\Pi]\!]+2D_{nn}[\![\mu]\!]+[\![\rho]\!] g z_\Sigma+S^*(\frac{1}{R_1}+\frac{1}{R_2}-\frac{2}{a}) = 0. \tag{3.8}$$

The dynamic pressure is of course an unknown which must be determined from the solution. This equation will be used in (4.4).

IX.4 STOKES FLOW AROUND A DROP OR BUBBLE

It is of interest here to consider the solution due to Hadamard and Rybczynski [Clift, Grace and Weber 1978; Happel and Brenner 1983] for the problem of a falling drop when the Reynolds numbers are small enough so that inertia may be neglected. The solution is also discussed in §4.9 of Batchelor [1970]. For numerical simulations on the problem at finite Reynolds numbers, see Dandy and Leal [1989].

When inertia is negligible, if we assume that the drop is spherical and is falling at its terminal speed, and match the shear stress and velocities at the interface, then the normal stress condition will be seen a posteriori to be automatically satisfied. Thus, a spherical drop falling at its equilibrium speed is a steady solution.

We begin by supposing that interfacial tension is large enough to keep the drop spherical against the deforming effect of the viscous forces. We use spherical polar coordinates $(r,\ \theta,\ \phi)$, with the spherical interface Σ being $r = a$. On Σ, $z = z_\Sigma = a\cos\theta$. We assume axisymmetry: $\partial/\partial\phi = 0$. It is convenient to introduce a stream function ψ such that

$$u_r = \frac{-1}{r^2\sin\theta}\frac{\partial\psi}{\partial\theta}, \quad u_\theta = \frac{1}{r\sin\theta}\frac{\partial\psi}{\partial r}. \tag{4.1}$$

The velocity and shear stress are made continuous at the interface and the kinematic condition is satisfied. Let U be the speed of the drop. It can be shown (see equation (4.9.5) of Batchelor [1970]) that the required solution is in the form

$$\psi = f(r)\sin^2\theta, \quad r \geq a, \tag{4.2}$$

$$\psi_d = f_d(r)\sin^2\theta, \quad r \leq a,$$

where

$$f(r) = Ar + Br^2 + \frac{D}{r},$$

$$f_d(r) = Er^4 + Fr^2,$$

$$A = -\frac{3Ua\,(\mu_d + \frac{2}{3}\mu)}{4\quad \mu_d + \mu}, \quad B = \frac{1}{2}U,$$

$$D = \frac{Ua^3}{4}\frac{\mu_d}{\mu_d+\mu}, \quad E = \frac{U}{4a^2}\frac{\mu}{\mu_d+\mu}, \quad F = \frac{-U}{4}\frac{\mu}{\mu_d+\mu}.$$

The pressure for Stokes flow is harmonic $\nabla^2\Pi = 0$ and the solution is given by

$$\Pi = \frac{aU\cos\theta}{r^2}\frac{\mu(\mu + \frac{3}{2}\mu_d)}{\mu_d+\mu}, \quad r \geq a, \tag{4.3}$$

$$\Pi_d = \frac{-5Ur\cos\theta}{a^2}\frac{\mu}{\mu_d+\mu}, \quad r \leq a.$$

The solution (4.2) and (4.3) is obtained by satisfying all the required conditions except the normal stress equation (3.8). It can be shown that the solution automatically satisfies

the normal stress condition. Equation (3.8) may be written on $z_\Sigma = a\cos\theta$ and $R_1 = R_2 = a$ as

$$-[\![\Pi]\!] + 2D_{rr}[\![\mu]\!] + [\![\rho]\!]ga\cos\theta = 0, \tag{4.4}$$

where

$$D_{rr} = \frac{\partial u_r}{\partial r}_{(r=a)} = \frac{-2\cos\theta}{a^2} f'(a) = \frac{-2U\cos\theta}{a}\frac{\mu}{\mu_d + \mu}, \tag{4.5}$$

and

$$[\![\Pi]\!] = (\Pi_d - \Pi)_{r=a} = \frac{-U\cos\theta}{a}\left(\frac{13\mu}{2} + \frac{\mu^2}{\mu_d}\right). \tag{4.6}$$

In equation (4.4), the interfacial tension term vanishes, so that it is not necessary to assume a priori that the effect of surface tension must be enough to keep the drop spherical. For example, a large air bubble rising in tar can take a spherical shape, even when the effect of interfacial tension cannot be dominant. Putting this all together, we get

$$\left(\frac{-3U\mu}{a}\frac{\mu + \frac{3}{2}\mu_d}{\mu_d + \mu} + [\![\rho]\!]ga\right)\cos\theta = 0. \tag{4.7}$$

This yields

$$U = \frac{1}{3}\frac{a^2 g}{\mu}(\rho_d - \rho)\frac{\mu + \mu_d}{\mu + \frac{3}{2}\mu_d}. \tag{4.8}$$

The analysis just given shows that if the flow is very slow, so that inertia may be neglected, the sphere is a solution for the shape of a drop falling at its terminal speed. At low Reynolds number, a solution is a slightly perturbed sphere [Taylor and Acrivos 1964]. There is numerical and experimental evidence to suggest that these solutions are stable to small disturbances [Koh and Leal 1990; Pozrikidis 1990] but not to large disturbances.

Huang and Joseph [1991] have extended the above result to the case in which a drop falls from rest under gravity. In this situation, we have the unsteady Stokes equation with gravity as the body force for the flows inside and outside the drop. Suppose the drop has a speed $U(t)$ in the direction of gravity. Then in a coordinate system moving with the drop, the governing equations are the continuity equation (3.4) and

$$\rho\frac{\partial \mathbf{u}}{\partial t} = -\nabla p - \rho(g - \dot{U}(t))\mathbf{e_z} + \mu\nabla^2\mathbf{u}. \tag{4.9}$$

We divide the pressure into three parts: $p = p^a + \Pi + p^s$, where p^s is the static pressure satisfying $[\![p^s]\!] = 2/a$, p^a is the pressure due to the body force, which can be found from $\nabla p^a = -\rho(g - \dot{U})\mathbf{e_z}$, and Π is the dynamical pressure, which will be determined with the solenoidal velocity $\mathbf{u}$ by

$$\rho\frac{\partial \mathbf{u}}{\partial t} = -\nabla\Pi + \mu\Delta\mathbf{u}. \tag{4.10}$$

Equation (4.10) holds in both fluids.

Assuming now that the flow is axisymmetric, we introduce a stream function as in (4.1). Equations (3.1) and (3.7) imply that $[\![u_\theta]\!]$, $[\![u_r]\!]$, $[\![\mu D_{r\theta}]\!]$ all vanish, and

$$-[\![\Pi]\!] + 2[\![\mu D_{rr}]\!] + [\![\rho]\!](g - \dot{U}(t))a\cos\theta + S^*\left(\frac{1}{R_1} + \frac{1}{R_2} - \frac{2}{a}\right) = 0, \tag{4.11}$$

where S^* is the surface tension coefficient and $\frac{1}{R_1}+\frac{1}{R_2}$ is the mean curvature of the surface.

It is concluded that the spherical bubble does not need interfacial tension to retain its shape when it is accelerating because the weight is momentarily greater than the drag. The proof will be as follows. First, we suppose that the surface tension is large enough to keep the spherical shape of the bubble: that is, we ignore equation (4.11) and enforce the other boundary conditions on the sphere. Then we show that this equation will automatically be satisfied without any condition on S^*.

Taking the curl of (4.10), we get the equation for the stream function $\psi(r,\theta,t)$:

$$\rho\frac{\partial}{\partial t}E^2\psi = \mu E^4\psi, \tag{4.12}$$

where

$$E^2 = \frac{\partial^2}{\partial r^2} + \frac{\sin\theta}{r^2}\frac{\partial}{\partial\theta}\left(\frac{1}{\sin\theta}\frac{\partial}{\partial\theta}\right).$$

We can separate variables:

$$\psi(r,\theta,t) = f(r,t)\sin^2\theta. \tag{4.13}$$

Then u_r can be written as $\tilde{u}_r(r,t)\cos\theta$, $u_\theta = \tilde{u}_\theta(r,t)\sin\theta$. From the equation

$$\frac{\partial\Pi}{\partial r} = \mu\left(\nabla^2 u_r - \frac{\partial u_r}{\partial r} - \frac{2}{r^2}\frac{\partial u_r}{\partial\theta} - \frac{2u_\theta}{r}\cot\theta\right) - r\frac{\partial u_r}{\partial t},$$

where

$$\nabla^2 = \frac{1}{r^2}\left(\frac{\partial}{\partial r}\left(r^2\frac{\partial}{\partial r}\right)\right) + \frac{1}{r^2\sin\theta}\frac{\partial}{\partial\theta}\left(\sin\theta\frac{\partial}{\partial\theta}\right),$$

we see that $\Pi(r,\theta,t)$ is of the form

$$\Pi(r,\theta,t) = \tilde{\Pi}(r,t)\cos\theta.$$

Hence,

$$D_{rr}(r,\theta,t) = \frac{\partial u_r}{\partial r} = \tilde{D}_{rr}(r,t)\cos\theta,$$

$$D_{r\theta} = \frac{1}{2}\left(r\frac{\partial}{\partial r}\left(\frac{u_\theta}{r}\right) + \frac{1}{r}\frac{\partial u_r}{\partial\theta}\right) = \tilde{D}_{r\theta}(r,t)\sin\theta.$$

Now let us compute the force acting on the spherical bubble by the outside fluid which, because of the symmetry, must be along $\mathbf{e_z}$. By Newton's law, the magnitude of this force is equal to the force acting on the outside fluid by the bubble. Hence,

$$\int \mathbf{e_z}\cdot[\![\mathbf{T}]\!]\cdot\mathbf{n}\,ds = 0, \tag{4.14}$$

where

$$[\![\mathbf{T}]\!] = (-[\![\Pi]\!] + [\![\rho]\!](g - \dot{U}(t))a\cos\theta))\mathbf{I} + 2[\![\mu\mathbf{D}(\mathbf{u})]\!],$$

$\mathbf{e_z} = \cos\theta\mathbf{e_r} - \sin\theta\mathbf{e}_\theta$, $\mathbf{n} = e_r$, and $\mathbf{I}$ is the unit matrix, and the integral is executed on the spherical surface.

Using all the above equations and $ds = 2\pi a^2 \sin\theta \, d\theta$, we get

$$2\pi a^2 \big(- [\![\tilde{\Pi}(a,t)]\!] + [\![\rho]\!](g - \dot{U}(t)a) + 2[\![\mu \tilde{D}_{rr}(a,t)]\!] \big) \int_0^\pi \cos^2\theta \sin\theta \, d\theta = 0. \tag{4.15}$$

Therefore,

$$-[\![\tilde{\Pi}(a,t)]\!] + [\![\rho]\!](g - \dot{U}(t)a) + 2[\![\mu \tilde{D}_{rr}(a,t)]\!] = 0.$$

This is just the sum of the first three terms of equation (4.11). Thus, if we can find a solution for $f(r,t)$, the proof is finished.

We introduce $V = a^2 g\rho/\mu$, a and V/g as scales for the velocity, length and time respectively, and Va^2 for $f(r,t)$. Then, using the same notation for the dimensionless variables, the initial value problem becomes

$$\frac{\partial}{\partial t} L^2 f = L^4 f, \qquad \text{for } r > 1;$$

$$\frac{\partial}{\partial t} L^2 f_d = L^4 f_d, \qquad \text{for } 0 < r < 1;$$

$$f(r,0) = f_d(r,0) = U(0) = 0,$$

$$f(1,t) = f_d(1,t) = 0,$$

$$[\![\frac{\partial f}{\partial r}]\!] = 0,$$

$$\frac{1}{r}\frac{\partial^2 f}{\partial r^2} - \frac{2}{r^2}\frac{\partial f}{\partial r} = m\left(\frac{1}{r}\frac{\partial^2 f_d}{\partial r^2} - \frac{2}{r^2}\frac{\partial f_d}{\partial r}\right),$$

$$f(r,t) \to -\frac{1}{2} r^2 U(t) \quad \text{as } r \to \infty,$$

and

$$d\dot{U}(t) = \left(-\frac{\partial^3 f}{\partial r^3} + \frac{2}{r}\frac{\partial^2 f}{\partial r^2} + \frac{2}{r^2}\frac{\partial f}{\partial r} + d - 1\right)\Big|_{r=1} + \frac{\partial^2 f}{\partial r \partial t}\Big|_{r=1},$$

where

$$d = \frac{\rho_d}{\rho} \quad \text{and} \quad m = \frac{\mu_d}{\mu}.$$

The system was solved for $f(r,t)$ and $U(t)$ by a finite element method. Graphs of $f(r,t)$ versus r for $m = 0.9$, $d = 0.95$ at two different times are given in figure 4.1. Graphs of the dimensionless $U(t)$ versus t for different parameters are given in figure 4.2. The terminal velocity of the drop is given by

$$\tilde{U} = \frac{2(1+m)(d-1)}{3(2+3m)}.$$

This is the dimensionless form of equation (4.8). Figure 4.2 shows that the unsteady solution $U(t)$ converges to $\tilde{U}$ as t approaches infinity.

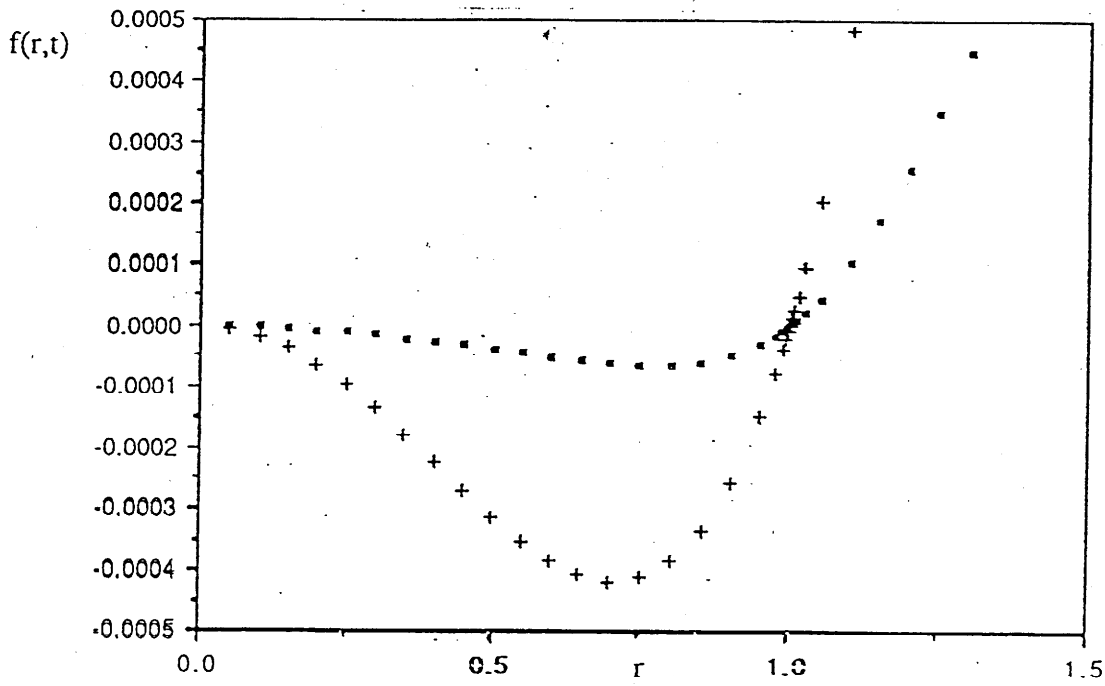

Figure 4.1 $f(r,t)$ vs r, $m = 0.9$ and $d = 0.95$: $(\bullet)$ $t = 0.11$, $(+)$ $t = 0.27$.

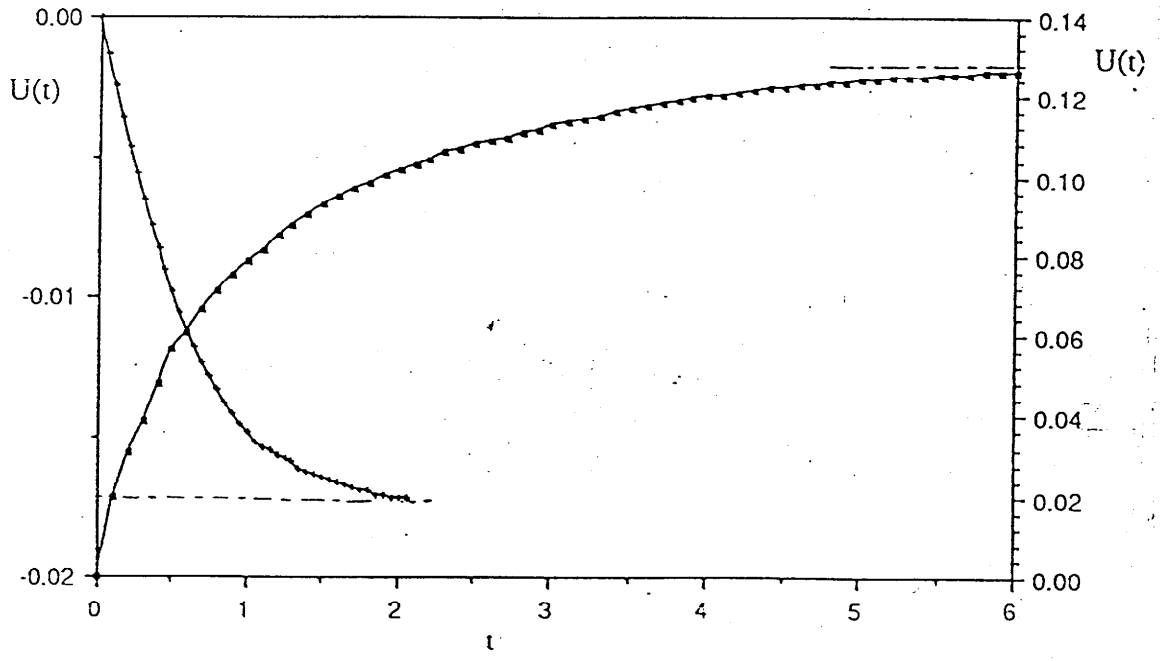

Figure 4.2 $U(t)$ vs t: (+) $m = 0.9$, $d = 0.95$, $\tilde{U} = -0.0172$; (•) $m = 0.4$, $d = 1.3$, $\tilde{U} = 0.1273$. Positive values of $U(t)$ are for falling drop and negative are for rising bubble.

IX.5 DIMENSIONLESS PARAMETERS

To identify dimensionless parameters, we scale lengths with a, the radius of the equivalent spherical drop or bubble with the same volume, and velocity with U to be specified later (see section IX.6). The normal stress balance at the interface (see section IX.3) shows that there are four forces at work: gravity, surface tension, inertia and viscosity.

The viscosity ratio

$$M = \frac{\mu_d}{\mu}, \tag{5.1}$$

where μ_d is the viscosity of the drop and μ is the viscosity of the ambient fluid, is very important.

The ratio of inertia to viscous forces is measured by the Reynolds numbers

$$R = \frac{Ua}{\nu}, \quad R_d = \frac{Ua}{\nu_d}, \tag{5.2}$$

where $\nu = \mu/\rho$, $\nu_d = \mu_d/\rho_d$. To form immiscible vortex rings, inertia is important because the drop will be close to a sphere if R and R_d are sufficiently small [Clift, Grace and Weber 1978].

The viscous part of the normal stress in the drop is scaled by $U\mu_d/a$ and in the exterior fluid by $U\mu/a$. The interfacial tension term in the stress balance is scaled by S^*/a. The ratio of the stress associated with interfacial tension to the viscous part of the normal stress in the outer fluid is

$$\frac{S^*}{\mu U} = \frac{J}{R}, \tag{5.3}$$

where

$$J = \frac{S^* a}{\nu^2 \rho}, \tag{5.4}$$

is Chandrasekhar's capillary number (used in his study of the capillary instability of a jet; see §111 of his book [1981]) for the outer fluid. Similarly, for the inner fluid we have

$$\frac{S^*}{\mu_d U} = \frac{J_d}{R_d}, \tag{5.5}$$

where

$$\frac{M J_d}{R_d} = \frac{J}{R}. \tag{5.6}$$

For a ring to form, the tendency for interfacial tension to keep the drop spherical should be overcome by the effect of viscosity to distort it. Thus, we expect to see rings when $M >> 1$ and $J/R << 1$.

The inertial part of the dynamic pressure for the outer fluid is scaled with ρU^2 and the drop with $\rho_d U^2$. The ratio of interfacial tension to inertia in the outside fluid is

$$\frac{(S^*/a)}{\rho U^2} = \frac{J}{R^2}, \tag{5.7}$$

and in the drop is

$$\frac{(S^*/a)}{\rho_d U^2} = \frac{J_d}{R_d^2}. \tag{5.8}$$

Obviously,

$$\frac{\rho_d}{\rho}\frac{J_d}{R_d^2} = \frac{J}{R^2}. \tag{5.9}$$

Since ρ and ρ_d do not differ greatly in our experiments, the ratio of interfacial tension to inertia is nearly the same in the outside fluid and the drop.

IX.6 PHYSICAL AND OTHER PROPERTIES

The physical properties are density, viscosity and interfacial tension. Other properties used in our discussion are the velocity U and the drop size a. First, we discuss the fluid properties.

Table IX.1 lists the fluids used in the experiments. The densities were measured using a Curtin Scientific hydrometer at approximately 21 degrees Celsius. The viscosities were measured using standard Cannon Fenske tube viscometers at approximately 21 degrees Celsius. Canola oil is also termed rapeseed oil. The glycerin listed is .99 pure USP glycerin. The percentages listed for golden syrup and glycerin are dilutions with water. Alconox is an industrial glass cleaner and is used as a surfactant with water. The interfacial tension S^* was measured with the spinning rod tensiometer.

TABLE IX.1

Fluid Properties

Fluid	Density (g/cm^3)	Kinematic Viscosity (cstokes)	Viscosity (g/cm sec)
Canola Oil	0.915	67	0.61
Glycerin	1.265	656	8.29
.95 Gly*	1.245	244	3.03
.91 Gly	1.240	113	1.40
.92 Golden Syrup	1.400	2606	36.49
Lyle's Golden Syrup	1.440	20804	299.58
Motor Oil 30W	0.886	316	2.80
Olive Oil	0.914	69	0.63
Palmolive Soap	1.05	238	2.50
Safflower Oil	0.920	51	0.47
Sesame Oil	0.920	64	0.59
Shell Research Oil	0.895	2037	18.23
Sil** 5cS	0.930	5	0.05
Sil 100cS	0.960	100	0.96
Sil 200cS	0.970	200	1.94
Sil 300cS	0.970	300	2.91
Sil 400cS	0.970	400	3.88
Sil 500cS	0.971	500	4.86
Sil 600cS	0.971	600	5.83
Sil 1000cS	0.971	1000	9.71
Sil 10000cS	0.975	10000	97.50
Sil 30000cS	0.975	30000	292.50
Soy Bean Oil	0.922	53	0.49
Water	1.000	1	0.01
Water+Alconox	1.080	33	0.36
Walnut Oil	0.925	51	0.47

* .95 Gly = 95 percent glycerin in 5 percent water

** Sil = Silicone oil with indicated viscosity

Baumann's experiments on vortex rings were carried out in a vortex ring box, a plexiglass tube three inches square and eight feet long. The top of Baumann's apparatus is open to allow introduction of the drop and the bottom is closed by a valve. The valve holds the host fluid in and allows the removal of the dropped fluids that collect at the bottom of the box. The plexiglass is clear to allow good visualization and photographic recording. The vortex ring box is back-lighted by two eight feet long fluorescent lights that are separated from the box by a translucent plexiglass sheet. The most recent experiments were carried out in a vortex ring tube, which differed from Baumann's apparatus in that it is a glass tube of circular cross-section with a three inch diameter. The tube is four feet long, and like Baumann's apparatus, it is open at the top, and closed at the bottom with a valve.

The method for introducing the drop into the vortex ring box is as follows. A 10 cc drop of the more dense fluid was carefully placed on top of the host fluid with a calibrated beaker. This gives

$$\frac{4}{3}\pi a^3 = 10\ cc \quad \text{or} \quad a = (2.39)^{1/3}\ cm\ = 1.34\ cm.$$

Care was taken to insure that the drop was not splashed or accelerated into the host fluid.

A parametric study of drop size was also carried out with volumes other than 10 cc. The results of these studies are summarized in figure 9.1.

The velocity scale we use to calculate the Reynolds numbers is U given by (4.8). The assumptions leading to this formula are that the fluid is a sphere falling at constant speed in Stokes flow, and that if the shear stress and velocity are matched at the interface, then the normal stress is automatically matched. The analysis does not say anything about what the drop would do if it were not falling at the terminal speed; for example, in the experiments, the drop starts at rest, some drops do not attain any steady speed, and moreover appear not to reach the speed predicted by this formula. It is difficult to decide *a priori* on a velocity scale because we do not have a formula for predicting the velocity as the drop changes shape. For each experiment, one could measure the maximum speed attained by the drop and use that as U, and this type of data is available for some of the experiments.

The velocity of the drop as it falls in the vortex ring box has been measured for some situations and found to be much smaller than the value from (4.8). Measurements of the velocity of a falling drop were made by recording the time it took for the drop to cross a six inch region of the box. Five such regions were selected to best capture the rate of fall at critical sections. The records were taken ten times for each region and the average velocity was calculated. Figure 6.1 shows the average velocity versus distance down the tube for three types of glycerin (e.g. 90% glycerin means 90% glycerin in 10 % water) and silicone oil falling in soy bean oil. (Rings were observed in the 100% glycerin case, but not in the other two cases, which happen to have higher velocities in the figure.)

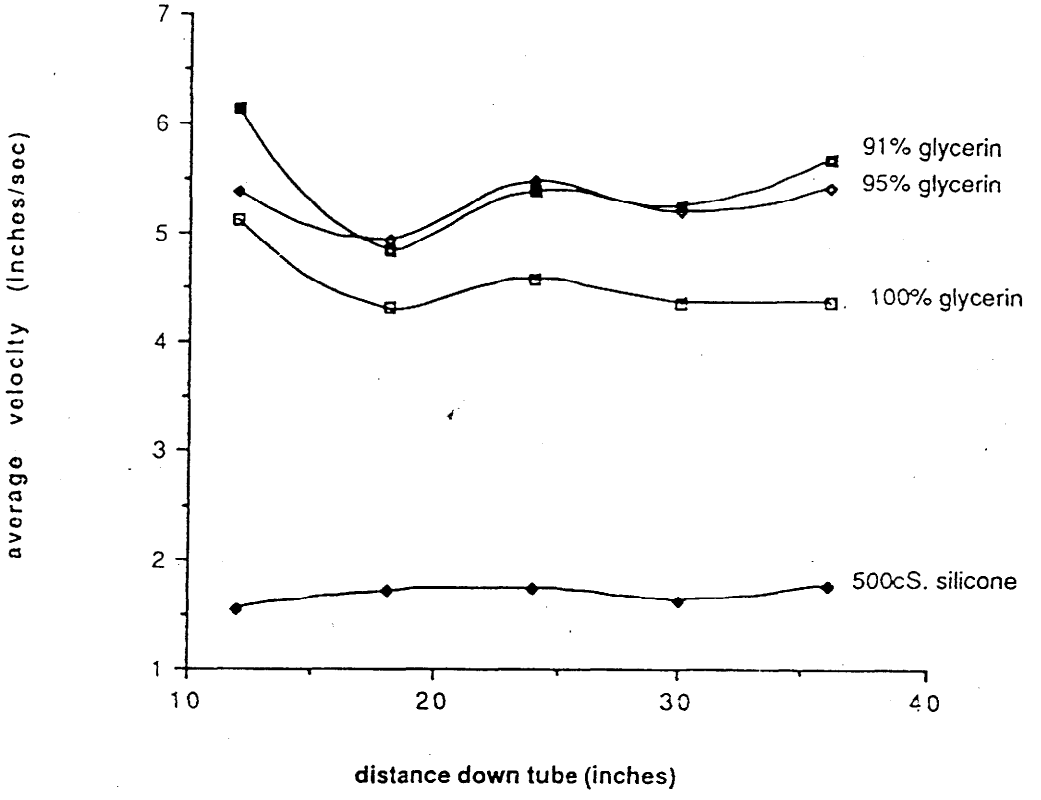

Figure 6.1 The average velocity versus distance down the vortex ring tube for the designated liquids falling in soy bean oil.

Take, for example, the data in this figure. Compared with this, the value of U from (4.8) is approximately 110 inches per second, which is about twenty times the actual average velocity. This is consistent with the notion that a spherical drop would fall faster than a flattened spheroid or a ring. The swings in the measured speed reflect the changes in the shape of the drop as it evolves into a ring and decays. We should therefore keep in mind when looking at the tables that the true Reynolds numbers are probably an order of magnitude less than those tabulated.

There are also situations where U from (4.8) turns out to be large which is inconsistent with one of the assumptions in the derivation of (4.8); but since Stokes drag is less than the actual drag at higher Reynolds numbers, we expect that the U is an upper bound on the actual maximum velocity. Thus, our tabulated values of J_d/R_d and J/R in the sequel underestimate the importance of surface tension, but consistently, so that they should probably be an order of magnitude larger than they are. This would imply that the switch in the behavior from ring formation to no ring is actually occurring at a value of J/R of order 1. This, in fact, is what one would expect.

It is interesting that the condition for ring formation (on M and J/R) appears to hold for the entire wide range of Reynolds numbers encountered in the experiments. Why? In the normal stress condition at the interface, the only term we have not really commented on above is the pressure term, which is multiplied by the Reynolds number R. It appears that this term does not affect the ability to give birth to a ring: indeed, the factor R

appearing there can be made to disappear just by changing the way the pressure is non-dimensionalized.

The formation of vortex rings always involves the breaking of a membrane, by poke-through or blow-out, and the breaking strength (toughness) of a membrane is very difficult to control, especially in silicone-vegetable oil systems. Paul Mohr repeated the experiments of Nick Baumann with good success except for the breaking of silicone-vegetable oil membranes. Mohr did some experiments with a contaminated safflower oil with various additives that Baumann used to complete his studies. We could never break a membrane in a silicone-contaminated safflower oil system (figures 7.5 and 8.2). The breaking strength of a membrane may be related to interfacial tension since we could get tough membranes to break by adding certain types of surfactants to the silicone oil (trace amounts of 97% dye, 3% Rhodamine B base powder in figure 8.3; trace amounts of Igepal in figure 8.4). We also had difficulty breaking membranes in a silicone-soy bean oil system, even when uncontaminated fluids were used. However, the oils used in the most recent experiments were not exactly the same as those used by Baumann, and it is possible that the newer oils had an interfacial tension large enough to prohibit vortex ring formation. As was the case for the contaminated oil system, rings were formed when the above mentioned surfactants were added to the silicone oil.

IX.7 DISTORTION OF THE SPHERICAL DROP

When viscous effects win over the effect of interfacial tension, a falling drop cannot maintain a spherical shape. Numerical solutions have been obtained by Dandy and Leal [1989] for steady streaming flow past an axisymmetric drop over a wide range of Reynolds numbers, interfacial tension, viscosity ratios and density ratios. Their results indicate that at lower Reynolds numbers, the shape of the drop tends toward an indented oblate shape with decreasing interfacial tension, and at higher Reynolds numbers the drop becomes more disk shaped with decreasing interfacial tension.

In our experiments, the drop is released at zero speed and undergoes accelerations and decelerations, so that the results mentioned above concerning steady motions cannot strictly be used to infer anything about what our drop is doing. Moreover, as mentioned in section IX.6, measurements of the drop speed indicate that it often does not reach the steady speed predicted by the formula (4.8). However, there are similarities with these analyses and what we have seen.

Figure 7.1 shows an indented oblate drop like those computed by Dandy and Leal at low Reynolds numbers (see, for example, their figure 3). Experimental observations suggest that the streamline pattern on the concave side of the cap is probably like that of figures 7.2; there are no points of separation or vortices in this guess about the underlying fluid dynamics. The suction in the cap, call it a wake, is large and small drops and even large drops are easily captured by the indented drop, as shown in figures 7.3, 7.4, 7.5 (a) and 8.1 (a). If the conditions are right, the drop in the wake will poke through the membrane spanning the indentation, as in figures 8.1 and 8.3, but if the membrane is tough, as in figures 7.5 and 8.2, the poke-through will fail.

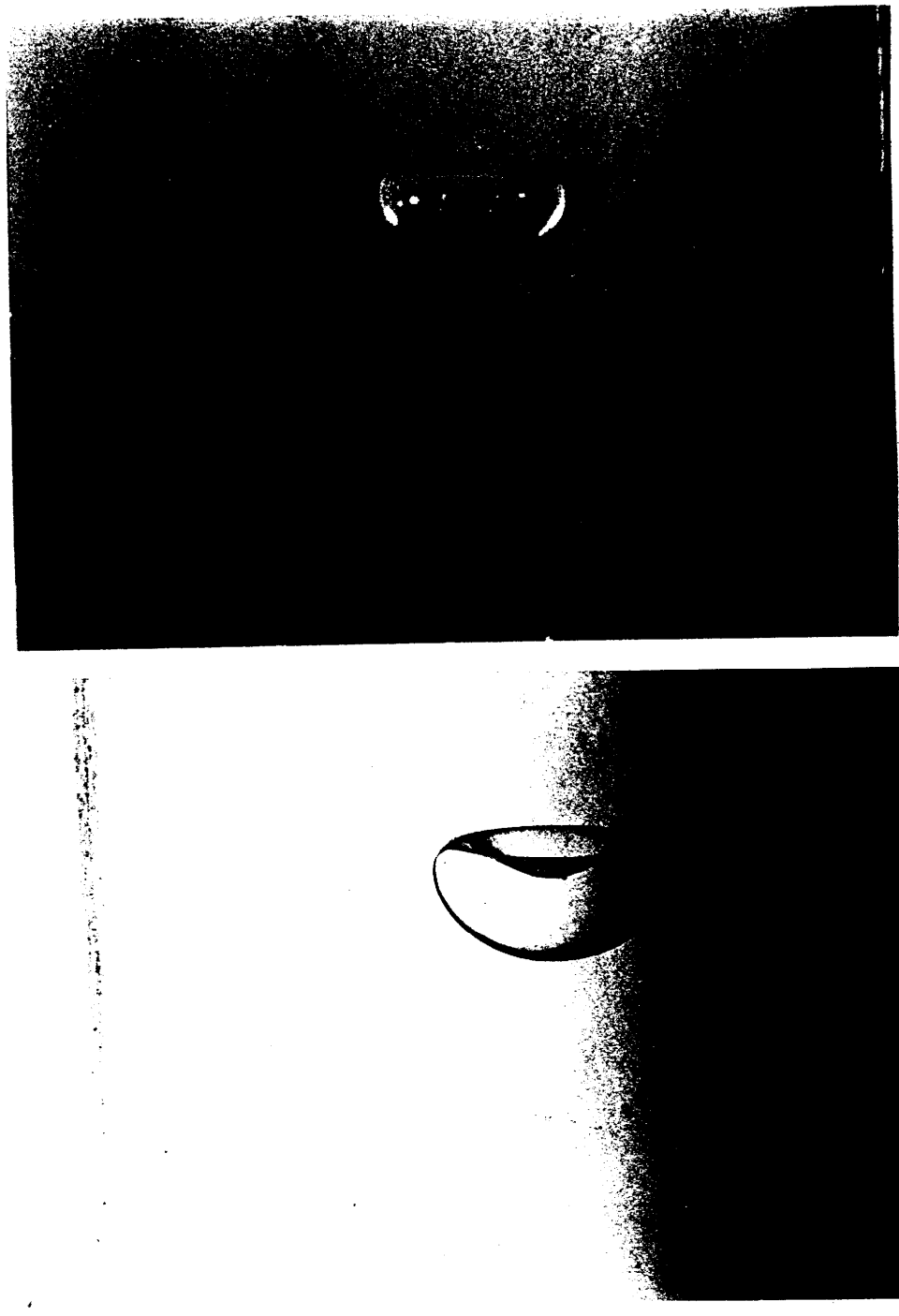

(a)

(b)

Figure 7.1 Indented oblate drops falling in safflower oil. (a) Water $M = 0.02$, $J = 4530$, $S^* = 3.39$ dyn/cm. Indentation never develops in water and oil systems without surfactants. (b) 500 cS silicone oil. These are the most common shapes when falling. The high viscosity drop develops a circulation which brings it closer to a vortex ring.

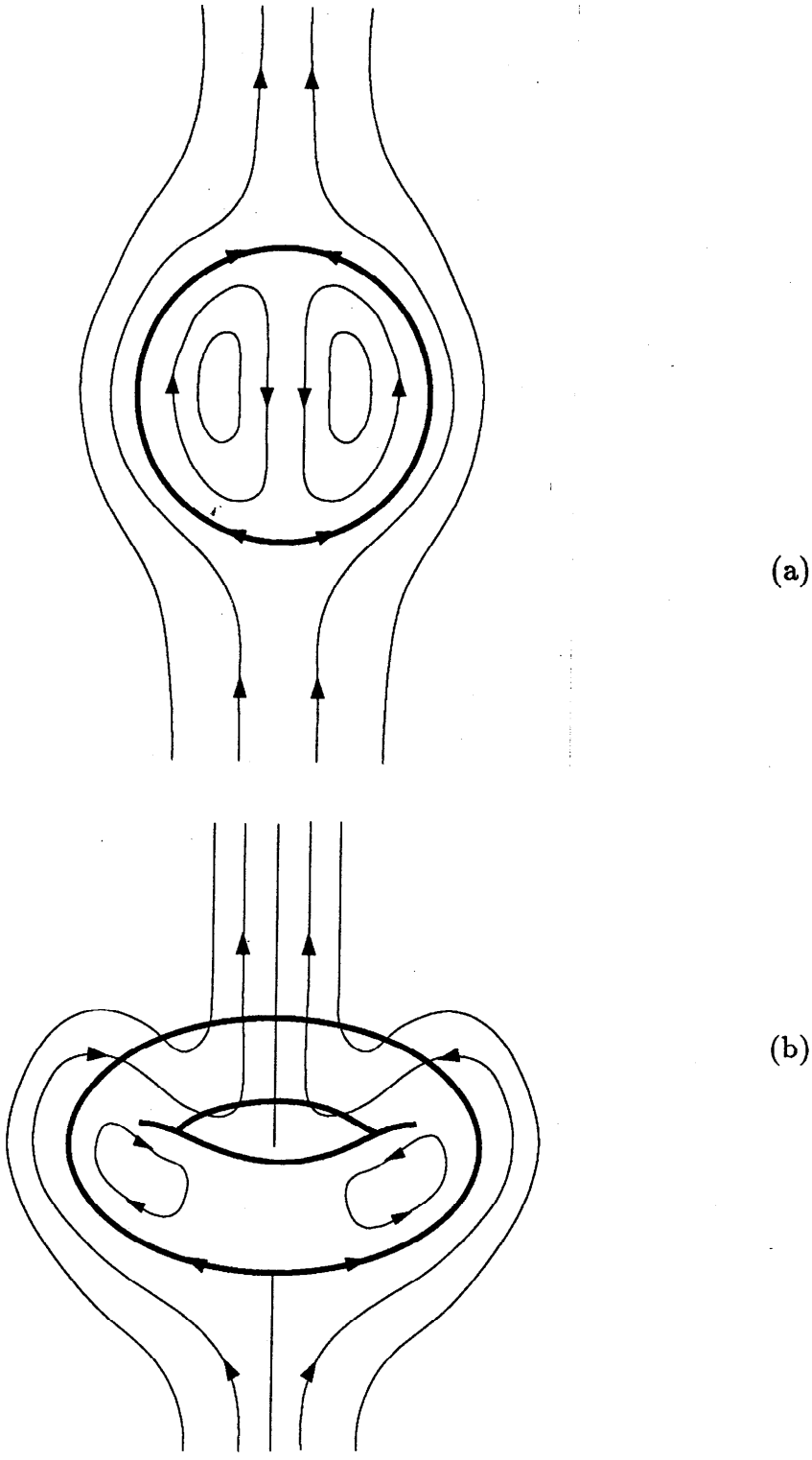

Figure 7.2 Development of vorticity in a drop falling from rest. The streamlines are sketched in a frame moving with the drops: (a) from experimental observations at sufficiently small velocity, (b) larger velocity.

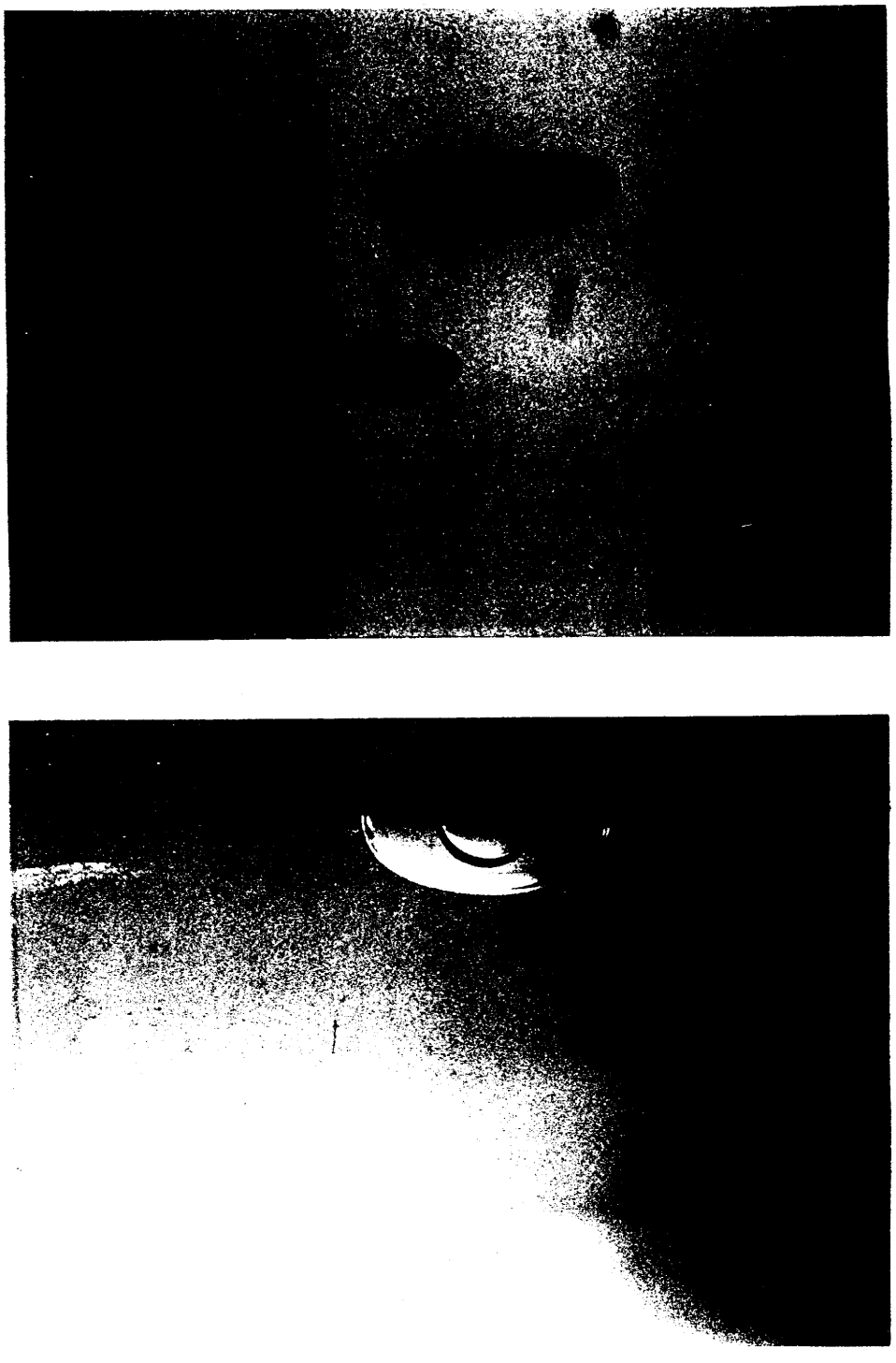

(a)

(b)

Figure 7.3 Spheres nested in the wake of an indented oblate drop. (a) Glycerin falling in soy bean oil $M = 16.9$, $J = 0.45$, $S^* = 18.45$ dyn/cm. (b) 500 cs silicone oil in contaminated safflower oil.

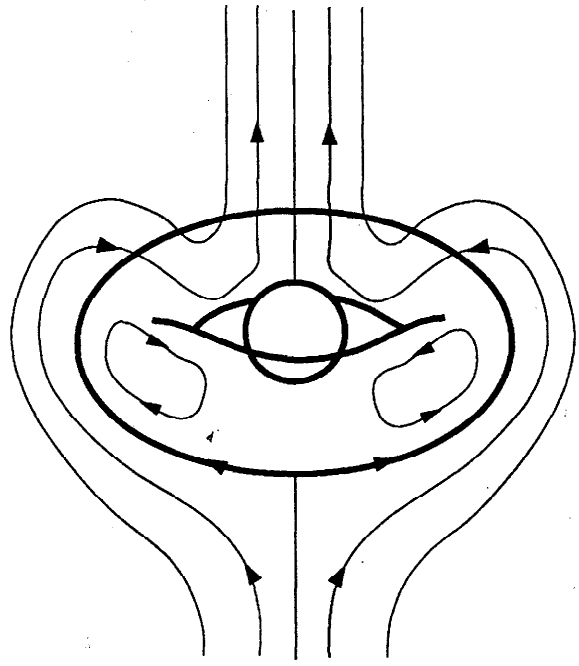

Figure 7.4 A streamline pattern for figure 7.3. The flow in the wake could pull out a tail from the nested sphere if the wake were strong as in figure 7.5 (b), or the surface tension weak as in the case of miscible liquids.

(a)

(b)

Figure 7.5 (a) - (b)

(c)

Figure 7.5 Failure of poke-through of captured drop of 1000 cS silicone oil in an indented oblate drop of the same silicone oil falling through contaminated safflower oil. (a) The captured drop is sucked strongly into the wake behind the oblate drop. There is a tail drawn out of the captured drop by the motion of safflower oil in the wake which reminds one of the tail behind drops in miscible liquids (cf. figure 2.2 (c)). (b) The drops are sucked into strong contact. (c) The captured drop decelerates under the restraining action of the silicone oil membrane on the oblate drop which never breaks.

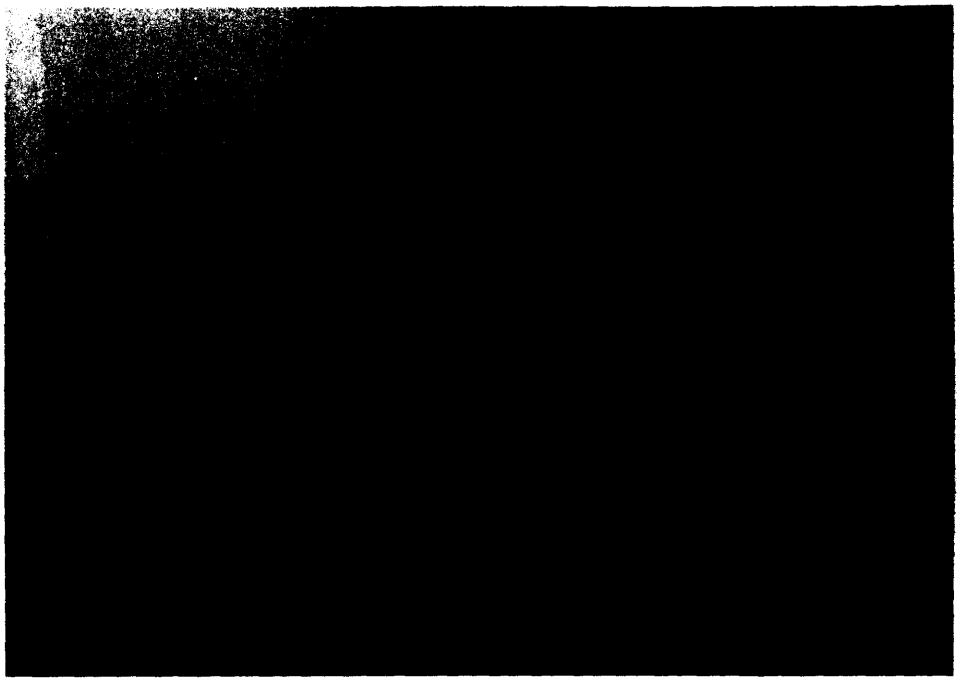

(a)

(b)

Figure 7.6 Crisco rising in a column of water with surfactant (Alconox). The value of interfacial tension has been reduced from 3.39 dyn/cm to 0.158 dyn/cm by the surfactant. The membrane does not break, despite the low tension. (a) A torus is formed inside the water bag. (b) The water in the torus is dragged out in the wake.

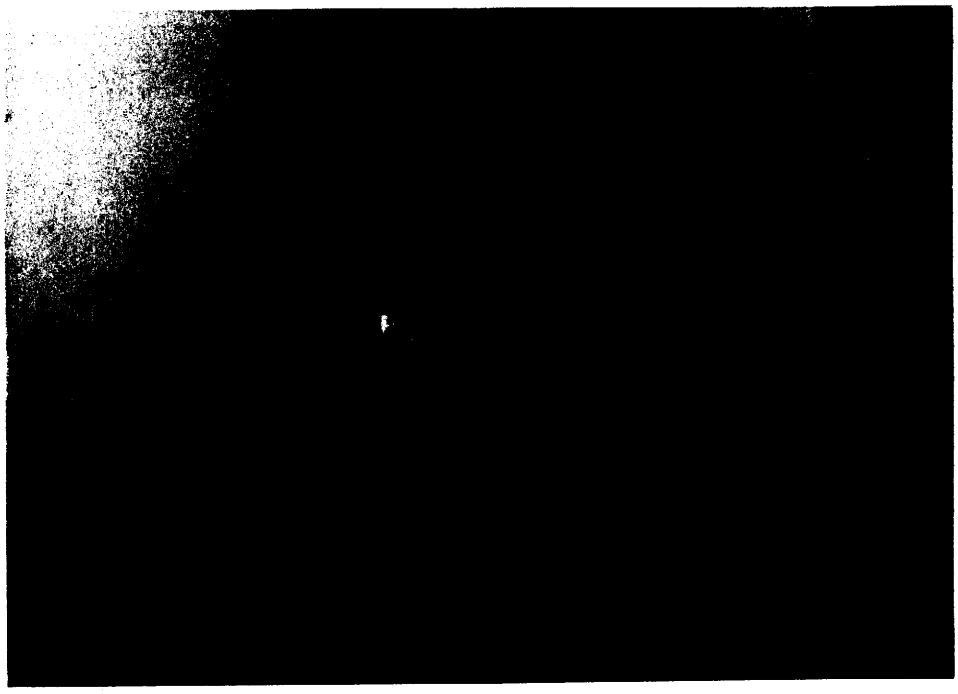

(c)

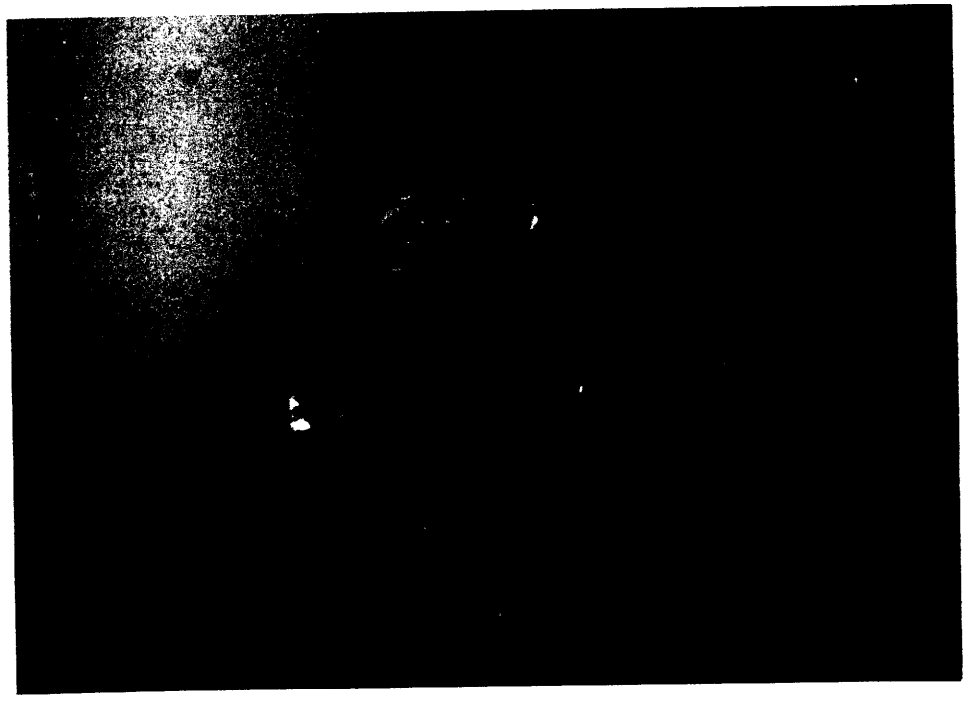

(d)

Figure 7.6 (c) - (d)

IX.8 FORMATION OF RINGS

If the conditions are right, if the drop is much more viscous than the host fluid ($M >> 1$) and the ratio J/R of interfacial to viscous forces is not too large, then the spherical drop will evolve toward a vortex ring. The entries in tables IX.2 to 4 for drops of silicone oils in soy bean oil exemplify these effects well. The viscosity of silicone oil can be varied through careful mixing without changing their density or surface tension appreciably. It was observed that when the viscosity of the drop was lower than a certain value (about 500 centistokes here), rings did not form. In particular, when the drop was less viscous than the bath, even with very low interfacial tension, rings did not form, as in figure 7.6.

Inertia alone will not cause a ring to form. Indented oblate drops like those shown in figure 7.1 are the most robust of the falling drops. If conditions are such that the viscous action of the host fluid can create a permanent circulation (like that sketched in figures 7.2 (b) and 7.4) of sufficient strength, the drop will begin to look like a ring, spanned by a membrane, as in figures 7.3, 7.4, 8.1 (a) and especially 8.2 (a). A free ring will form only if the membrane breaks. The membrane may or may not break. If it breaks, it does so either by poke-through of a smaller drop caught in the wake as in figures 8.1 and 8.2, or by blow-out. Blow-out can best be understood by the failure of blow-out shown in figure 8.2 (a). Blow-out can occur only if the membrane is very weak as in miscible liquids or in low interfacial tension systems like those shown in figures 8.4 and 8.5.

Vortex rings are unstable; whether or not the membrane has broken, the ring will expand rapidly. The rapid extension is a universal characteristic of the instability. If a membrane remains and no drop rests in the wake to poke through, the membrane will stretch and either rupture or fold as in figure 8.2 (b).

Due to capillarity, draining, or other causes, bulges develop on the ring; these fall faster than the rest of the ring, and fluid drains rapidly to the heavy bulges, exacerbating the instability. This instability can be considered as a manifestation of the Rayleigh-Taylor instability of the heavy fluid into the light, when the heavy fluid has the shape of a vortex ring. In our experiments, the draining almost always occurs at just two points of the ring, more or less at opposite points on the ring as in figures 2.2 (d), 2.3 (f), 8.1 (d) and 8.3 (f). This type of instability scenario can occur even for ring-like structures like the one shown in figure 8.2 (a) in which the membrane does not break and it leads to the folded ring shown in figure 8.2 (b). The heavier places fall faster and the ring bends and breaks into drops.

(a)

(b)

Figure 8.1 Poke-through of 1000 cS silicone oil in safflower oil $M = 19.8$, $J = 0.03$, $S^* = 2.41$ dyn/cm. (a) Silicone oil spheres nested in the wake of an indented oblate drop of the same oil. (b) Poke-through leads to a vortex ring. (continued)

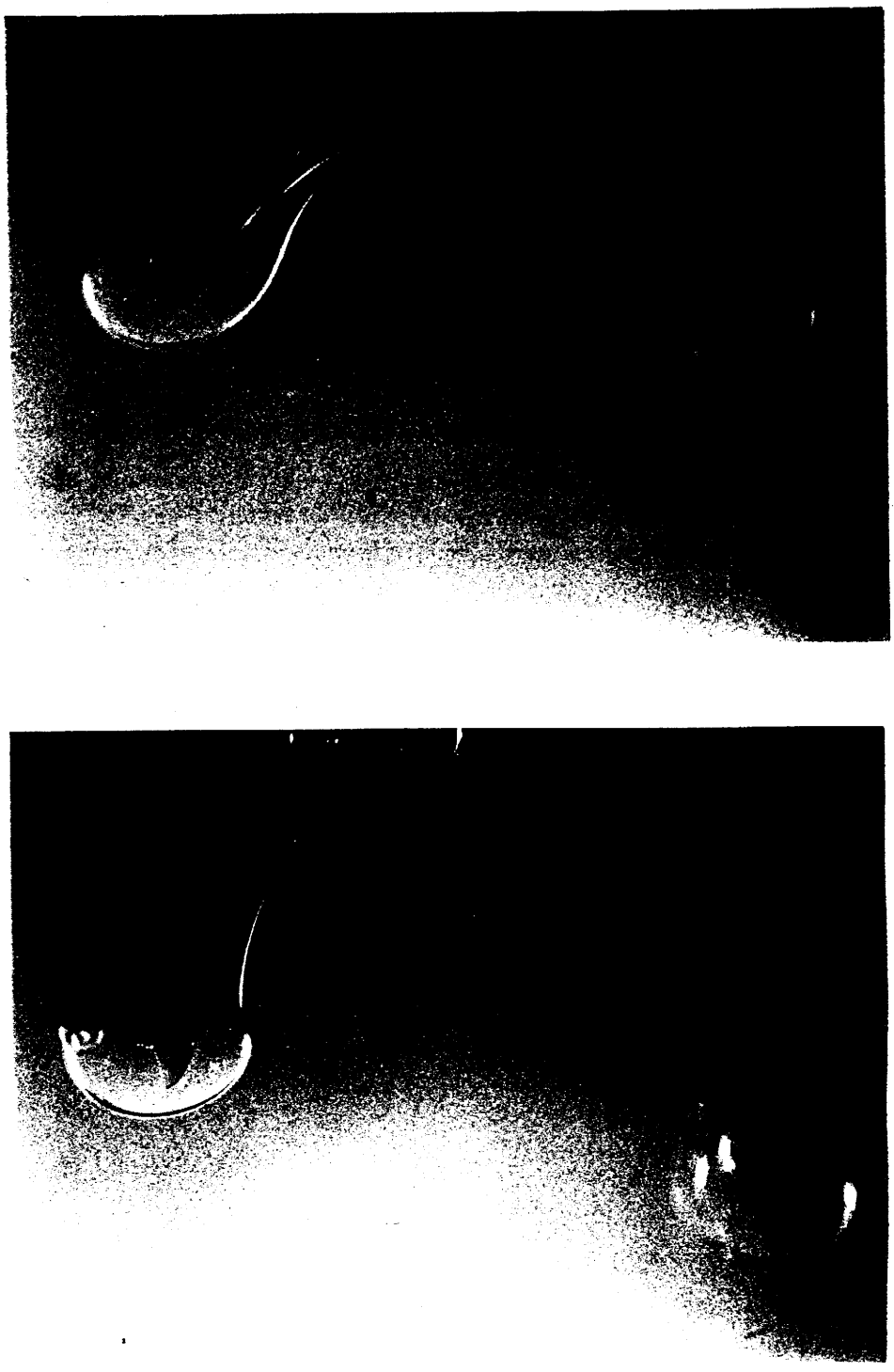

(c)

(d)

Figure 8.1 (c) - (d) (c) Vortex ring (Rayleigh-Taylor) instability is the rapid expansion of the ring diameter and the draining of the oil into the falling bulges. (d) Two new indented oblate drops form from the falling bulges in a replication of the dynamic sequence.

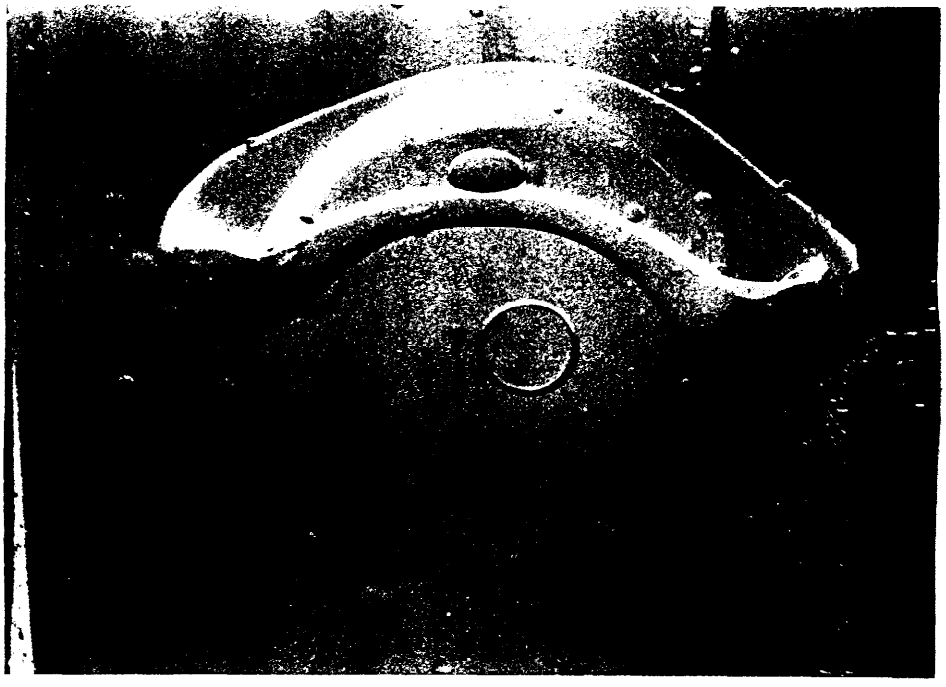

(a)

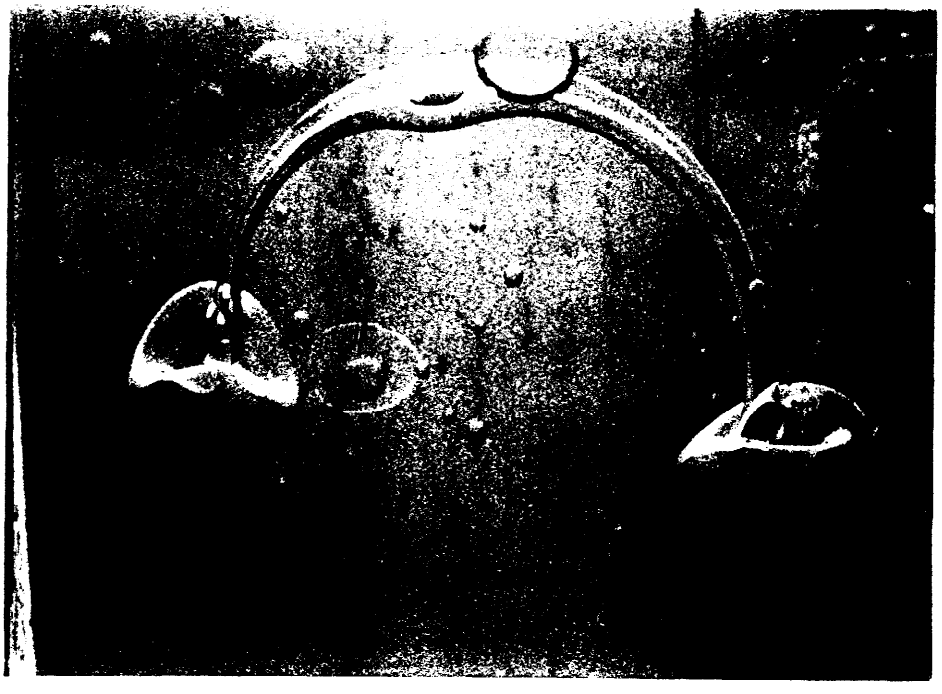

(b)

Figure 8.2 1000 cS silicone oil falling in contaminated safflower oil. (a) A vortex ring with circulation has developed but a tough membrane spans the ring. (b) The ring is unstable in the usual way (Rayleigh-Taylor instability) forming the characteristic drops (cf. figure 8.1 (d)), but the membrane breaks.

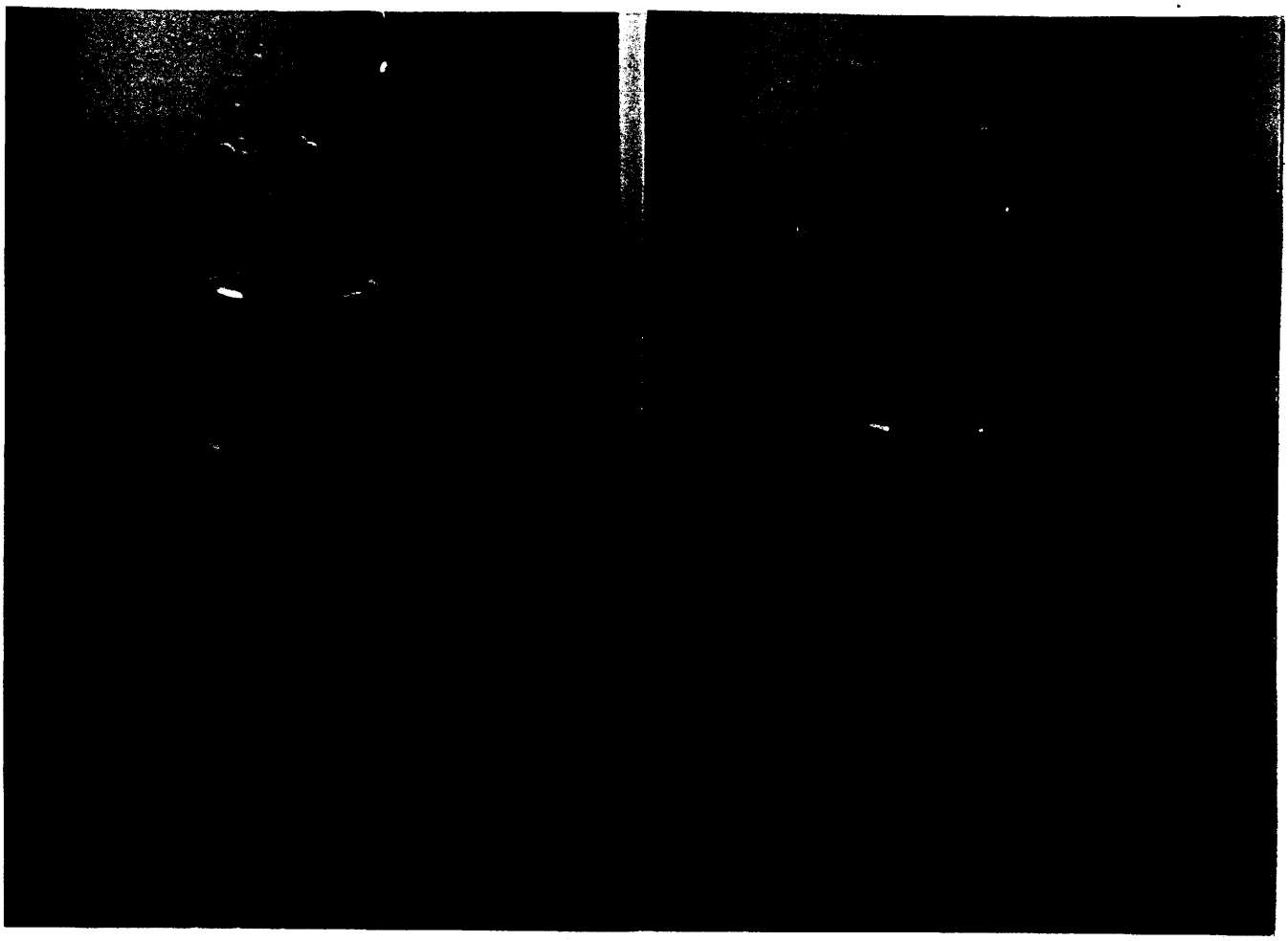

(a) (b)

Figure 8.3 Ring formation in 1000 cS silicone oil with a surfactant falling in soy bean oil. The surfactant is a trace amount of 97% dye with 2% Rhodamine B base powder. (a) One indented oblate sphere accelerates in the wake of another; (b) they come close. (c) Poke-through: the large ring loses its membrane. (d) The small ring never pokes through; it retains the oblate indented shape. (e) Beginning of the two-lobe instability of the Rayleigh-Taylor type. (f) The instability can be compared with 8.2 (b) where the membrane does not break and with the miscible ring in figure 2.2 (d).

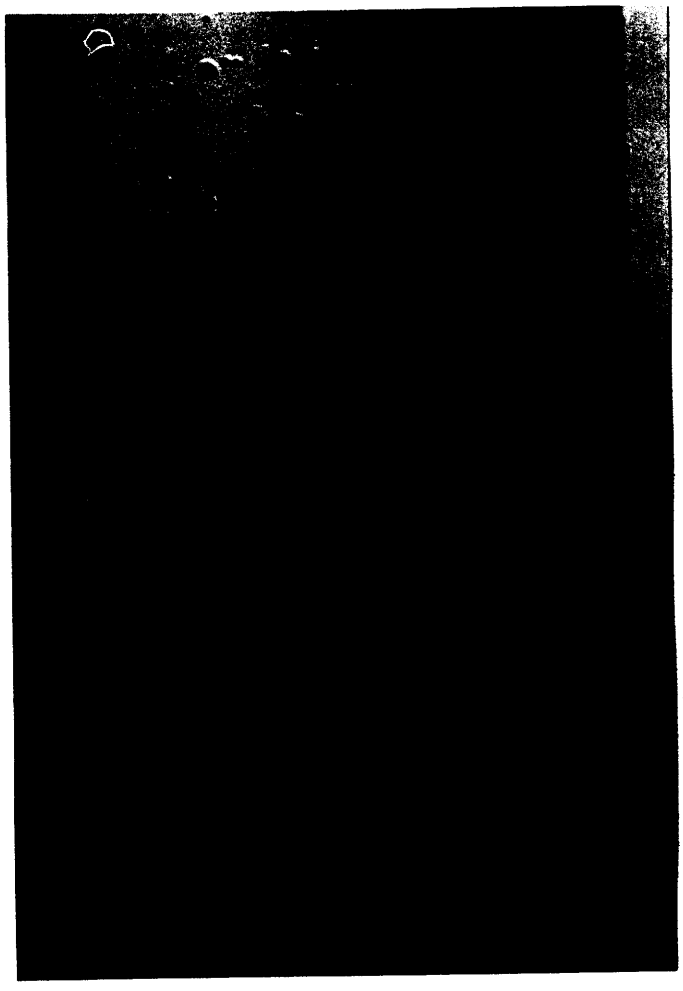

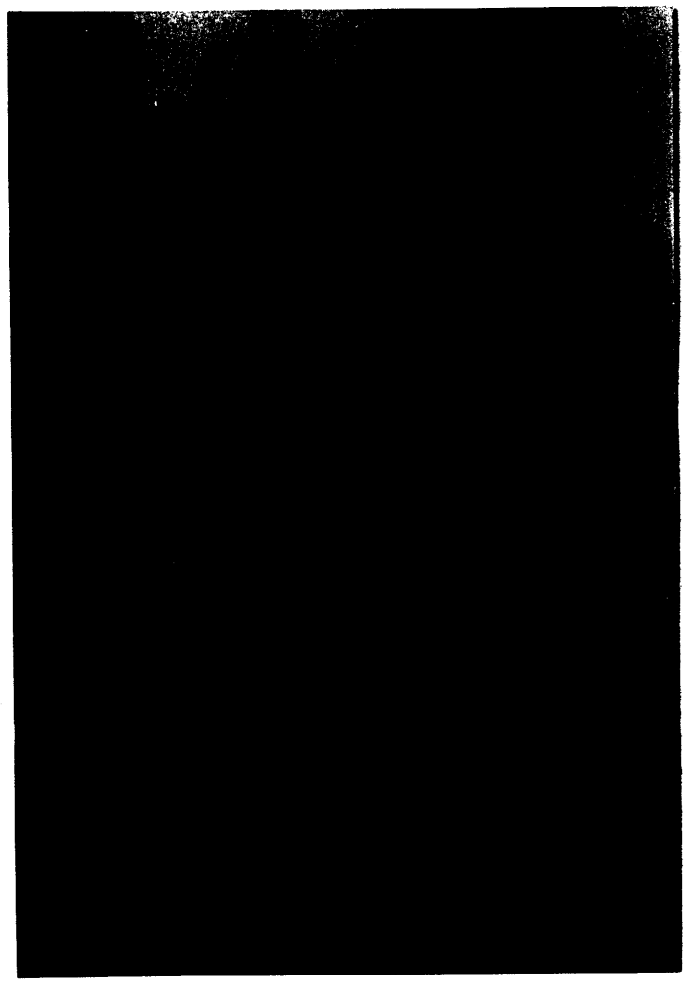

(c) (d)

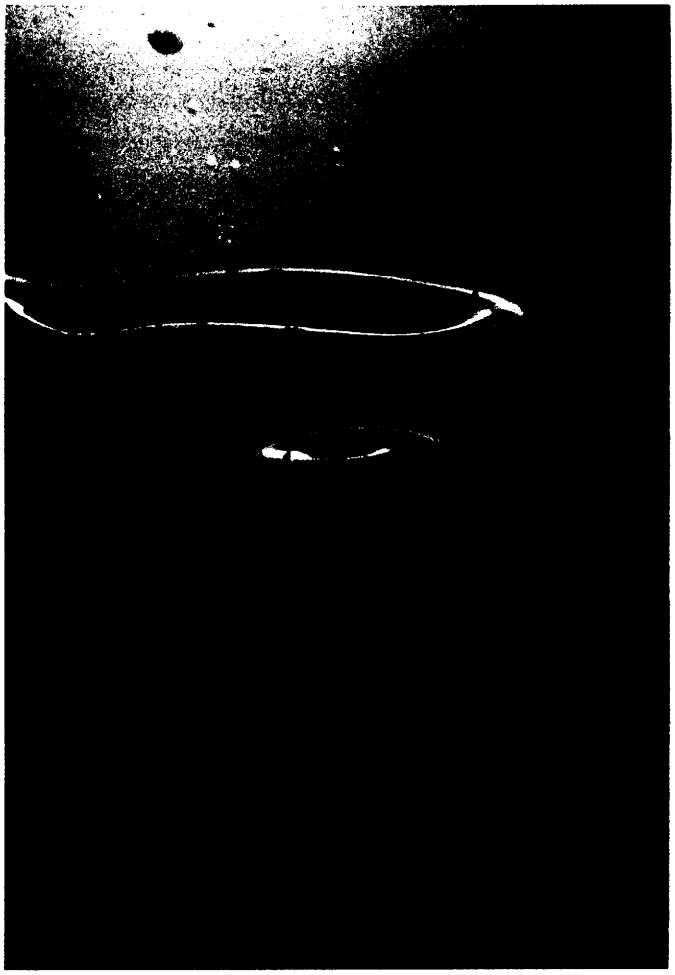

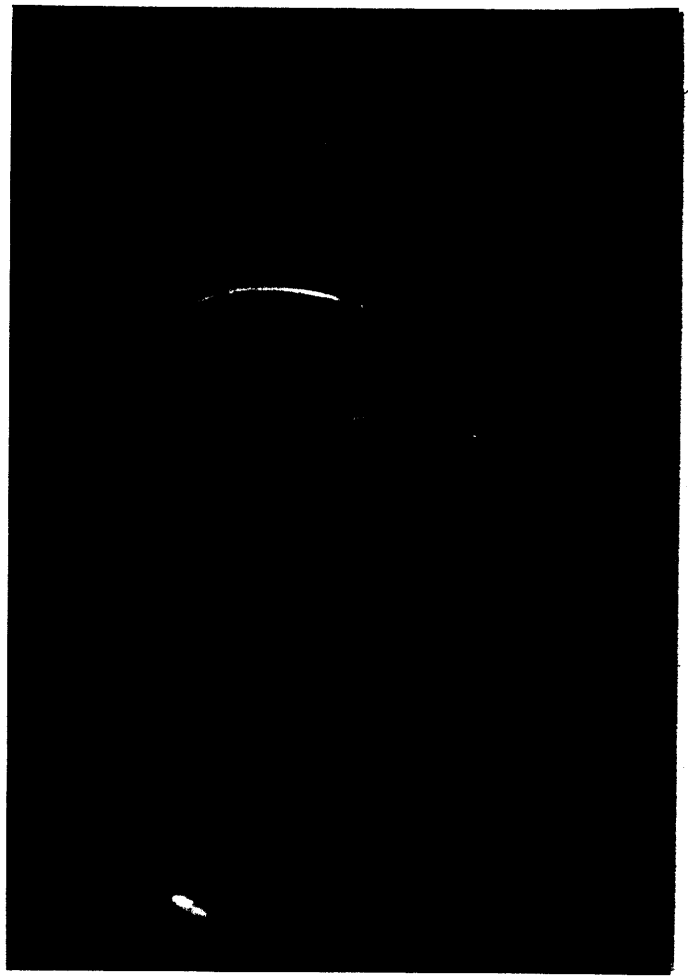

(e) (f)

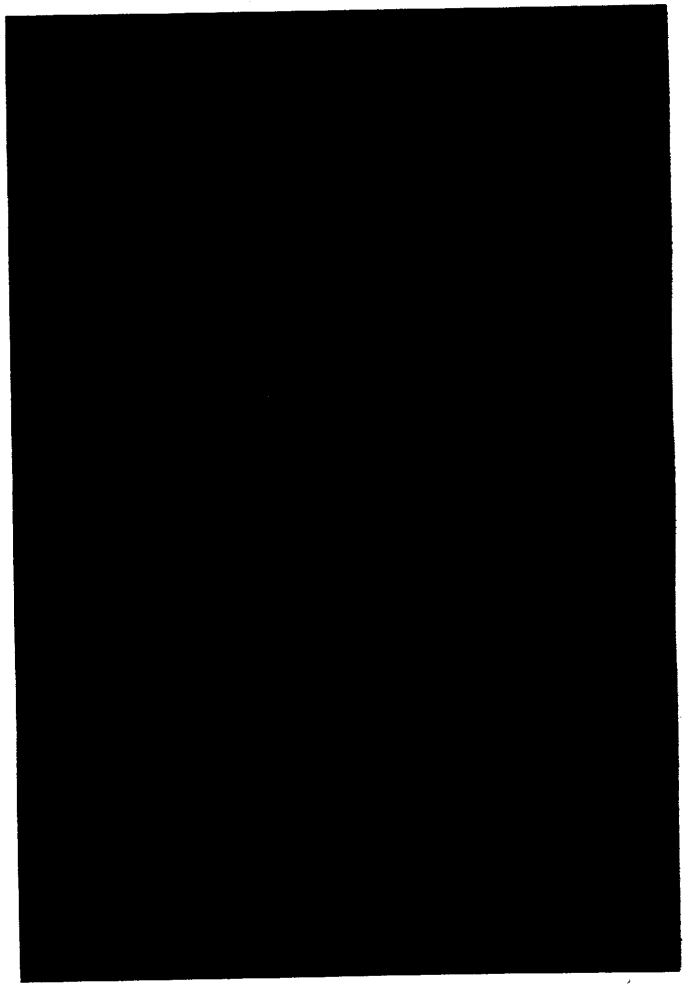

Figure 8.4 Vortex ring of 1000 cS silicone oil with trace amounts of surfactant (Igepal) falling in soy bean oil after blow-out.

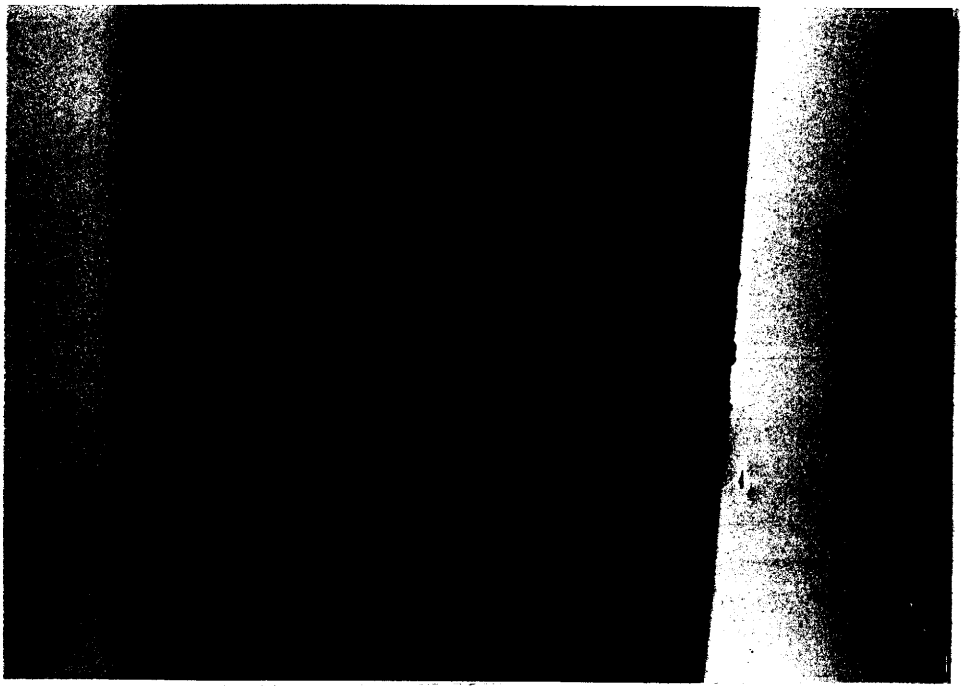

Figure 8.5 Vortex ring of dyed glycerine falling in soy bean oil after blow-out.

O'Brien [1985], in reviewing her own work and that of Stuke [1954], noted that the number of bulges which develop on the ring depends on the Reynolds number and is two for Reynolds numbers of order one or less. Basically, we observed only two bulges even at Reynolds numbers of order 100, with some very rare exceptions. Perhaps the number of bulges on the ring is related to capillary breakup and is strongly influenced by the value of interfacial tension. We saw many bulges when soap was added to water in soy bean oil (see the last entry of table IX.2). This interpretation is also suggested by the closely similar instability in miscible liquids reported by O'Brien [1961], in which case the lack of surface tension promotes the formation of many more nodules around the ring, the ring breaks into many drops, and those drops subsequently repeat the cycle and there is a vortex cascade [Thomson and Newall 1885]. Surface tension can keep subsequent drops spherical if they are small enough, and thus inhibits the cascade.

The effect of the wall on the drop and ring needs further study [Amarakoon, Hussey, Good and Grimsal 1982]. For example, when a ring approaches a wall of the apparatus, it expands considerably before touching it. Also, experiments done with a vortex tube of smaller diameter show that the walls inhibit ring formation. Observations about the way a ring behaves (in the miscible case) at a variety of boundaries is reported by Northrup [1912].

The dynamics leading to formation of vortex rings is not well understood. Data presented in the next section show that rings form from drops started from rest when the

viscosity of the drop is relatively great and the interfacial forces do not dominate viscous forces.

A falling drop is relentlessly sheared by the host fluid, but only small portions of the host fluid come under the influence of the falling drop, and these only momentarily. If we move with the drop, we can think that we have a uniform flow around the drop as in figure 7.2 (b), and this picture is also suggestive of why circulations develop in the drop and not in the host fluid. The flow around the ring would, in the case where the ring fluid is very viscous, resemble that of figure 2.1 (a), where the flow is analogous to the rigid-body rotation of figure 2.1 (b) and would then be almost potential flow, with potential flow at infinity (uniform flow), and the vorticity is localized to the interface region between the fluids.

IX.9 TWO-FLUID SYSTEMS THAT DO AND DO NOT FORM VORTEX RINGS

We used formula (4.8) to compute the velocity of a falling drop (with a= $(2.39)^{1/3}$) and rising bubble (with volume 5 cc, a= $(1.19)^{1/3}$) and evaluated many of the dimensionless parameters defined in section IX.5. The parameters are listed in tables IX.2, 3 and 4. Parameters which are not set down explicitly in these tables can be computed readily from the listed values. Table IX.2 tabulates the systems that were observed to form rings. The other two tables list the two-fluid pairs that were observed not to form rings.

We find that to form a ring, it is necessary that the drop fluid be much more viscous than the host fluid. Another criterion which appears to be necessary is that the effect of interfacial tension should be smaller than viscous effects, which may be expressed as

$$\frac{J}{R} < O(1), \tag{9.1}$$

where the notation is defined in (5.4) and (5.6). The last column of table IX.2 is comfortably in agreement with (9.1). However, the velocity U used to compute R was computed from (4.8) and the true J/R may be an order of magnitude larger than in the table. A very dramatic illustration of the importance of J/R and M is exhibited by data for Palmolive soap dropped in soy bean oil (a ring forms; see last entry of table IX.2) and water dropped in soy bean oil (a ring does not form). Palmolive soap is essentially water modified with a surfactant which reduces the interfacial tension enough to move J/R down to a sufficiently small value. The viscosity of Palmolive soap is greater than that of water and this alters M such that the combination of J/R and M produces a vortex ring. The evolution of the ring in this soapy solution is exceptionally rapid and the torus breaks up rapidly into small bubbles, as in the case of miscible liquids.

TABLE IX.2

Systems that form vortex rings

System	$\Delta\rho$ (g/cm^3)	$\Delta\nu$ (cS)	S^* (dyn/cm)	U (cm/sec)	R_d	ρ_d/ρ	M	J_d/R_d	J/R
Gly/Soy	0.343	606	18.45	278.5	57	1.37	16.9	.008	.135
500cS Sil /Soy	0.049	447	1.68	40.3	11	1.05	9.9	.008	.079
Gly /Canola	0.350	589	35.78	227.5	46	1.38	13.6	.02	.272
500cS Sil /Canola	0.056	433	2.33	37.0	10	1.06	8.0	.01	.080
Gly /Olive Oil	0.351	588	10.50	242.0	49	1.38	13.2	.005	.066
500cS Sil /Olive Oil	0.057	431	3.10	58.0	16	1.06	7.7	.01	.077
Gly /Safflower	0.345	606	15.65	291.5	59	1.38	17.6	.006	.106
500cS Sil /Safflower	0.051	450	7.44	43.6	12	1.06	10.3	.03	.309
Gly /Walnut Oil	0.340	605	39.51	285.8	58	1.37	17.6	.02	.352
500cS Sil /Walnut Oil	0.046	449	4.15	39.1	10	1.05	10.3	.02	.206
Gly /Sesame Oil	0.345	592	15.20	216.3	44	1.38	14.1	.008	.113
500cS Sil /Sesame Oil	0.051	436	3.40	34.9	9	1.06	8.2	.02	.164
500cS Sil /Soy	0.049	447	1.68	40.3	11	1.05	9.9	.008	.079
600cS Sil /Soy	0.049	547	2.68	40.1	9	1.05	11.9	.01	.119
1000cS Sil/Soy	0.049	947	2.41	39.7	5	1.06	19.8	.006	.119
10000cS Sil/Soy	0.053	9947	3.29	42.3	0.6	1.06	199.0	.0008	.159
30000cS Sil/Soy	0.053	29947	6.49	42.3	0.2	1.06	597.0	.0005	.298
Golden Syrup/Soy	0.518	20751	42.20	413.3	2.7	1.56	611.4	.0003	.183
.92Gold. Syrup/Soy	0.478	2553	28.46	382.6	19.6	1.52	74.47	.002	.149
Palmolive /Soy	0.128	185	18.10	108.0	61.0	1.14	5.10	.0006	.003

(continued)

Gly denotes 100 percent glycerin; .95Gly denotes 95 percent glycerin in 5 percent water; Shell denotes Shell Research Oil; Sil denotes silicone oil with the indicated viscosity; Soy denotes soy bean oil. The difference $\Delta\rho$ denotes (density of dropped fluid) — (density of host fluid); $\Delta\nu$ denotes (viscosity of dropped fluid) — (viscosity of host fluid): this difference is negative in some of the systems in the tables.

Table IX.3 displays systems that do not form vortex rings. The data show that a modification of the fluids will switch a system that forms a vortex ring to one that does not. An example is the glycerin and soy bean oil system. When 9 percent water is added to glycerin, the resulting diluted solution will not form a vortex ring because the viscosity ratio M has decreased and J/R has increased to the borderline level. A similar adjustment was made for golden syrup by adding water.

TABLE IX.3

Systems that do not form vortex rings

System	$\Delta\rho$ (g/cm^3)	$\Delta\nu$ (cS)	S^* (dyn/cm)	U (cm/sec)	R_d	ρ_d/ρ	M	J_d/R_d	J/R
.95 Gly /Soy	0.323	194	13.43	269.8	148	1.35	6.2	.02	.124
.91Gly /Soy	0.318	63	11.49	277.3	328	1.34	2.9	.03	.87
Water /30W Motor Oil	0.114	315	9.22	23.7	3172	1.13	0.004	38.85	.156
Water /Shell	0.105	2036	42.14	3.4	450	1.12	0.0005	1251	.625
Gly /Shell	0.370	1381	27.83	10.3	2	1.41	0.45	.34	.153
500cS Sil /Shell	0.076	1537	5.82	2.2	0.6	1.08	0.27	.53	.143
5cS Sil /Soy	0.008	-48	1.14	9.2	245	1.01	0.10	2.7	.27
100cS Sil /Soy	0.038	47	2.75	34.1	46	1.04	2.0	.08	.16
200cS Sil /Soy	0.048	147	2.16	40.9	28	1.05	4.0	.03	.12
300cS Sil /Soy	0.048	247	2.71	40.2	18	1.05	5.9	.02	.118
400cS Sil /Soy	0.048	347	2.67	39.7	13	1.05	7.9	.02	.158
Water /Soy	0.078	-52	3.39	92.3	12337	1.08	0.02	.37	.074
Water+ Alconox/Soy	0.158	-20 (continued)	4.64	156.0	632	1.17	0.73	.08	.056

.60Gold. Syrup/Soy	0.342	-27.5	7.42	341.0	1788	1.37	0.659	.07	.046

Table IX.4 lists systems where bubbles of the less dense liquid were released and left to rise through the more dense liquid. In each case, an oil was released into water. No vortex rings were observed. The related case of air bubbles released into water has been shown to yield rings (see figure 7 of Walters and Davidson [1963]). The case of 12500 centistoke silicone oil was inconclusive because the silicone oil showed an affinity for the plexiglass box.

TABLE IX.4
Systems of injected bubbles

System	S^* (dyn/cm)	ρ_d/ρ (μ_d/μ)	U	R_d (cm/sec)	M	J_d/R_d	J/R
100cS Sil /Water	24.67	0.96	984	1043	96	0.03	2.88
12500cS Sil/Water	27.11	0.975	621	5.3	12188	0.0004	4.8
Soy Oil /Water	3.39	0.922	1917	3829	49	0.004	0.196
30W Motor Oil/Water	9.22	0.886			280		
Olive Oil /Water	16.42	0.914	2119	3257	63	0.012	0.72

In figure 9.1, we display the results of a study of drop size on the distance required for ring formation. This distance decreases monotonically with volume and seems to asymptote to some small value less than 15 inches for large volumes.

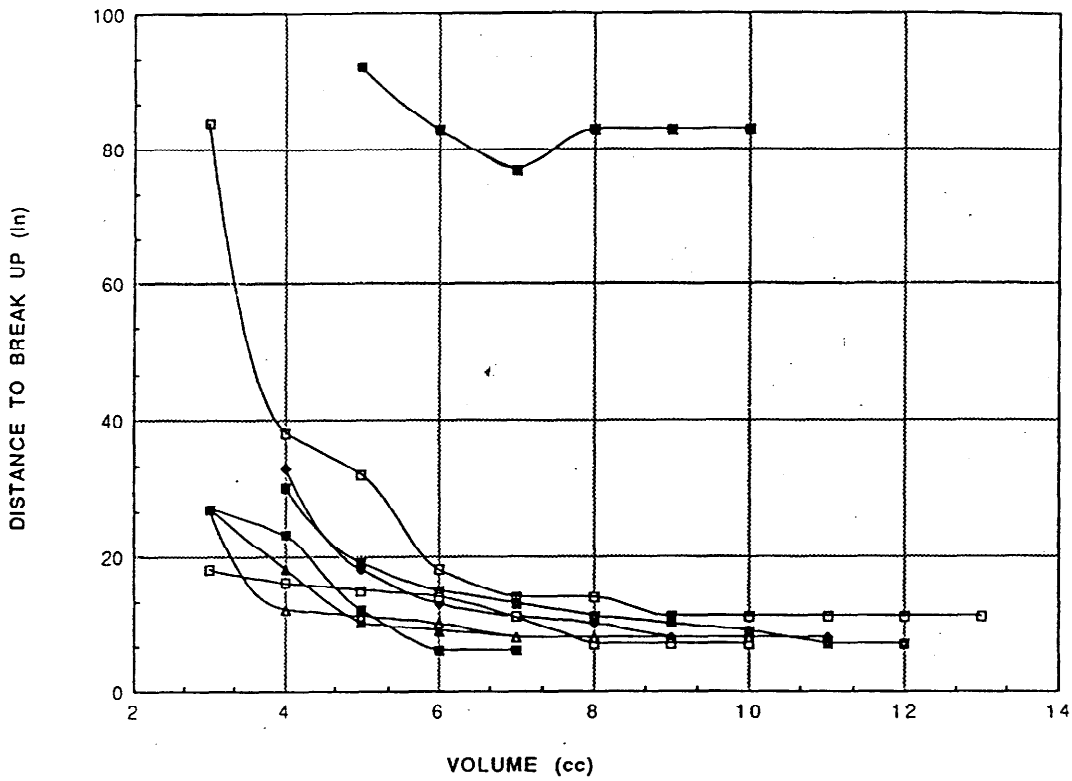

Figure 9.1 Distance travelled by a falling drop before a vortex ring forms as a function of drop volume. The formation of the ring occurs when the membrane spanning the ring breaks.